The Astrophysical Journal, 700:1732–1749, 2009 August 1 doi:10.1088/0004-637X/700/2/1732

GEODYNAMICS AND RATE OF VOLCANISM ON MASSIVE EARTH-LIKE PLANETS

E. S. Kite[1,3], M. Manga[1,3], and E. Gaidos[2]
[1] Department of Earth and Planetary Science, University of California at Berkeley, Berkeley, CA 94720, USA; kite@berkeley.edu
[2] Department of Geology and Geophysics, University of Hawaii at Manoa, Honolulu, HI 96822, USA
Received 2008 September 12; accepted 2009 May 29; published 2009 July 16

ABSTRACT

We provide estimates of volcanism versus time for planets with Earth-like composition and masses 0.25–25 $M_{\oplus}$, as a step toward predicting atmospheric mass on extrasolar rocky planets. Volcanism requires melting of the silicate mantle. We use a thermal evolution model, calibrated against Earth, in combination with standard melting models, to explore the dependence of convection-driven decompression mantle melting on planet mass. We show that (1) volcanism is likely to proceed on massive planets with plate tectonics over the main-sequence lifetime of the parent star; (2) crustal thickness (and melting rate normalized to planet mass) is weakly dependent on planet mass; (3) stagnant lid planets live fast (they have higher rates of melting than their plate tectonic counterparts early in their thermal evolution), but die young (melting shuts down after a few Gyr); (4) plate tectonics may not operate on high-mass planets because of the production of buoyant crust which is difficult to subduct; and (5) melting is necessary but insufficient for efficient volcanic degassing—volatiles partition into the earliest, deepest melts, which may be denser than the residue and sink to the base of the mantle on young, massive planets. Magma must also crystallize at or near the surface, and the pressure of overlying volatiles must be fairly low, if volatiles are to reach the surface. If volcanism is detected in the 10 Gyr-old τ Ceti system, and tidal forcing can be shown to be weak, this would be evidence for plate tectonics.

Key words: planetary systems – planets and satellites: general – planets and satellites: individual (COROT-7b, HD 40307 b, HD 40307 c, HD 40307 d, Gl 581 b, Gl 581 c, Gl 581 d, Gl 876 d, HD 181433 b, HD 69830 b, HD 69830 c, 55 Cnc e, GJ 674 b)

1. INTRODUCTION

Theory predicts the existence of rocky planets having 1–10 Earth masses (e.g., Ida & Lin 2004). Planets in this mass range are now being detected (Rivera et al. 2005), and next-decade observatories, such as the *James Webb Space Telescope* and *Giant Magellan Telescope*, may be able to detect any atmospheres. A planet's atmosphere will consist of gas (1) accreted from the nebula, (2) degassed during impact accretion, and (3) degassed during subsequent geologic activity. Point (1) will depend on the lifetime of the nebula, whereas (2) and (3) will depend on the volatile abundance of material (Elkins-Tanton & Seager 2008a), and all will be modified by atmospheric escape. Very large planets far from their parent star will retain primitive gas, but smaller planets closer to their parent star will not. Loss rates vary between gases, so planetary atmospheres could be a mixture of gases left over from the initial atmosphere, and those replenished by volcanism. Thermal emission phase curves gathered from extrasolar planets can set bounds on atmospheric mass. Spectral detection of atmospheric constituents with short photochemical lifetimes, such as SO_2, would require an ongoing source—most likely, volcanic degassing.

Volcanism results from partial melting of the upper mantle. (Planetary mantles can cool convectively without volcanism—present-day Mercury is almost certainly an example). Partial melting occurs when the adiabat crosses the solidus. Assuming that the adiabat is steeper than the solidus, this requires that the potential temperature of the mantle T_p exceed the zero-pressure solidus of mantle rock (e.g., peridotite; Figure 1(a)):

$$T_p = T_{m,r} - P_r \frac{\partial V}{\partial S} \geqslant T_{\rm sol}(0), \quad (1)$$

where $T_{m,r}$ is the mantle temperature evaluated at some reference pressure P_r, $\frac{\partial V}{\partial S}$ is the adiabat, potential temperature is defined as the temperature a parcel of solid mantle would have if adiabatically lifted to the surface, and $T_{\rm sol}$ is the solidus, evaluated here at zero pressure. On planets with plate tectonics, the thickness of the crust (the crystallized melt layer) is a convenient measure of the intensity of volcanism. The rate of crust production is the product of crustal thickness, plate spreading rate, and mid-ocean ridge length. The pressure at the base of the crust is the product of crustal thickness, the planet's surface gravity, and crustal density. A reasonable approximation to the pressure at the base of the crust is the integral of the fractional-melting curve from great depth to the surface (Figure 1(a)).

Venus and Mars lack plate tectonics: their mantles are capped by largely immobile, so-called "stagnant lid" lithospheres, which cool conductively. Because mantle cannot rise far into the stagnant lid, melting can only occur if the temperature at the base of the stagnant lid exceeds the local solidus of mantle rock:

$$T_{m,r} - (P_r - P_{\rm lith})\frac{\partial V}{\partial S} \geqslant T_{\rm sol}(P_{\rm lith}), \quad (2)$$

where $P_{\rm lith} = \rho_{\rm lith} g Z_{\rm lith}$ is the pressure at the base of the stagnant lid, $\rho_{\rm lith}$ is the lithospheric density, g is the gravity, and $Z_{\rm lith}$ is the stagnant lid thickness. This is a more stringent condition than Equation (1) if the adiabat is steeper than the solidus (Figure 1(b)). Io shows yet another style of rocky-planet mantle convection: magma pipe cooling.

Previous studies have examined both rocky planet atmospheres and massive-Earth geodynamics. Elkins-Tanton & Seager (2008a) estimate the mass and composition of super-Earth atmospheres degassed during accretion. Complementary to that study, we emphasize long-term geological activity. There is disagreement over whether plate tectonics will operate on massive

[3] Center for Integrative Planetary Science, University of California at Berkeley, Berkeley, CA, USA.

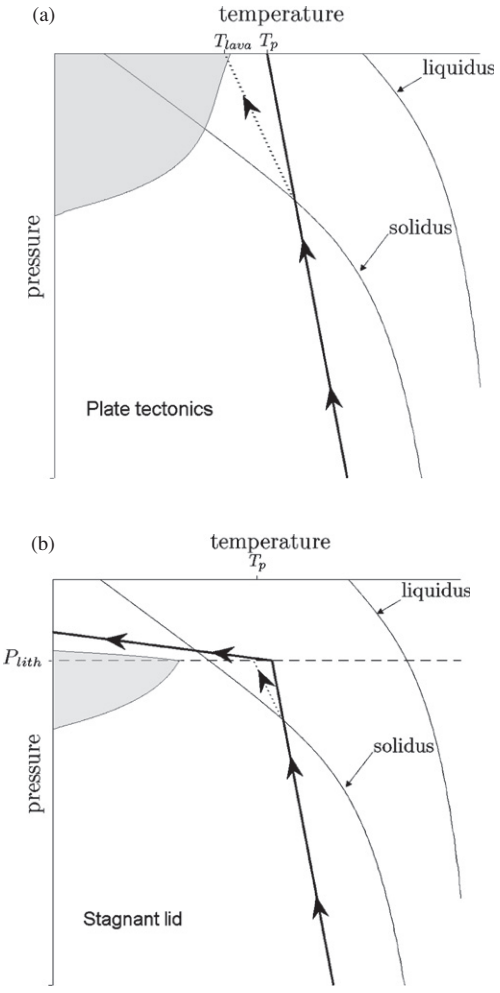

Figure 1. Sketches of pressure–temperature paths for passively upwelling mantle, and resulting melt fraction. In each sketch, the shaded area corresponds to the partial melt fraction as a function of pressure. (a) Plate tectonics. Thick solid line is the adiabatic decompression path for solid mantle. Actual path taken by upwelling mantle, traced by arrows, differs above the solidus because of latent heat of fusion. (b) Effect of a stagnant lid, whose base corresponds to the dashed line. Ascending mantle tracks the conductive geotherm within the lid (arrowed path). Melt generated at $P < P_{\rm lith}$ in the stagnant lid case is a small fraction of total melt, and we ignore it in this paper.

planets. One previous study uses scaling arguments to argue that higher gravity favors subduction (Valencia et al. 2007). Another study shows that subduction might never begin if the yield stress of old plate exceeds the stresses imposed by mantle convection (O'Neill & Lenardic 2007). We do not consider yield stresses in this paper. Instead, we analyze five possible volcanism-related limits to plate tectonics, tracing the consequences in more detail than the paper of Valencia et al. (2007). The approach of Papuc & Davies (2008) is most similar to that taken here. We differ from Papuc & Davies (2008) in that we neglect the pressure dependence of viscosity, use more realistic melting models, and account for energy advected by magma.

Here we examine (1) the history of partial melting on planets with either plate tectonics or stagnant lid convection, and (2) the effect of melting and crust production on the stability of plate tectonics. Our method is given in Section 2. We use three different melting models to compute the intensity of volcanism for massive Earth-like planets of different ages. Our results are given in Section 3, for both plate tectonic (Section 3.2) and stagnant lid (Section 3.3) modes of mantle convection. We also trace the implications of galactic cosmochemical evolution for heat production and planetary thermal evolution (Section 3.4). We find that results differ greatly depending on the mode of convection. Massive Earths with plate tectonics will produce melt for at least as long as the age of the Galaxy, but stagnant lid planets will not. In Section 4, we analyze the effect of melting on the style of mantle convection. We show that plate buoyancy is likely to be a severe problem and may be limiting for plate tectonics. In Section 5, we relate our results to atmospheric degassing and discuss the possible suppression of degassing (and, perhaps, melting) by the higher ocean pressures expected on massive Earth-like planets. Finally, in Section 6, we summarize our results, justify our approximations and model limitations, and compare our results to solar system data.

2. MODEL DESCRIPTION AND INPUTS

We use a model of internal structure (Section 2.1) to set boundary conditions for a simple model of mantle temperature evolution (Section 2.2), which in turn forces a melting model (Section 2.3). Greenhouse-gas regulation of surface temperature could allow melting and degassing to feed back to mantle thermal evolution (e.g., Lenardic et al. 2008), but we neglect this. Throughout, we assume whole-mantle convection. Rather than attempt to predict exoplanet properties solely from basic physics and chemistry, we tune our models to reproduce the thickness of oceanic crust on present-day Earth.

2.1. Radius and Mantle Depth

Given our assumption of whole-mantle convection, we need to know only the mantle's outer and inner radii. The crust is thin, so the top of the mantle is $\approx$ the planet's radius, R. Valencia et al. (2006) propose the scaling $R/R_\oplus = (M/M_\oplus)^{\sim 0.27}$. Here, we use instead the "modified polytrope" of Seager et al. (2007) (their Equation (23)) to set planet radius. However, we take $R/R_\oplus = (M/M_\oplus)^{\sim 0.25}$ in our scaling relationships (13), (14), and (21). To find the core–mantle boundary (CMB) radius for the Seager et al. (2007) scaling, we set mantle mass $M_{\rm mantle} = 0.675 M_{\rm planet}$ and numerically integrate inward using a pure magnesioperovskite mantle composition, a fourth-order Burch–Murnaghan equation of state, and material properties from Seager et al. (2007). CMB pressure is calculated to be 1.5 Mbar for 1 $M_\oplus$, and 2.9 (6.9, 14, 40) Mbar for 2 (5, 10, 25) $M_\oplus$.

2.2. Thermal Model

For a convecting mantle with a mobile lithosphere, if heat is generated solely by mantle radioactivity and is equal to heat lost by cooling at the upper boundary layer,

$$Q = \frac{M_{\rm mantle}}{A} \sum_{i=1}^{4} H_0(i) e^{-\lambda_i t} = Nu \frac{k(T_m - T_s)}{d} \quad (3)$$

$$Nu \approx \left(\frac{g\alpha(T_m - T_s)d^3}{\kappa \nu(T) R a_{\rm cr}} \right)^{\beta} \quad (4)$$

$$\nu(T) = \nu_0 e^{(A_0/T_m)} = \nu_1 e^{(-T_m/T_v)}, \quad (5)$$

where Q is the lithospheric heat flux, A is the planet's surface area, H is the radiogenic power per unit mass, i = 1–4 are the principal long-lived radioisotopes (^{40}K, ^{232}Th, ^{235}U, ^{238}U), λ is the decay constant, t is the time, Nu (Nusselt number) is the dimensionless ratio of total heat flow to conductive heat flow, k is the thermal conductivity, T_m is the mantle temperature, T_s

Table 1
Radioisotope Data: Half-Lives, Specific Power W, and Concentrations $[X](i)$ (ppb) After 4.5 Gyr

Parameter	^{40}K	^{232}Th	^{235}U	^{238}U	Reference
$t^{1/2}$ (Gyr)	1.26	14.0	0.704	4.47	
Specific power ($\times 10^{-5}$ W kg^{-1})	2.92	2.64	56.9	9.46	
Concentrations					
"Mantle"	36.9	124	0.22	30.8	Turcotte & Schubert (2002)
"Undepleted Earth"	30.7	84.1	0.15	21.0	Ringwood (1991)
CI chondrites	71.4	29.4	0.058	8.1	Anders & Grevesse (1989)
EH chondrites	147.8	2.8	5.8	13.0	Newsom (1995)

Note. $H_i = [X](i)W_i$.

Table 2
Parameters Used in Interior and Thermal Models

Parameter	Symbol	Value	Units	Reference
Thermal expansivity, mantle	α	3×10^{-5}	K^{-1}	1
Thermal conductivity	k	4.18	W m^{-1} K^{-1}	1
	β	0.3		1
Thermal diffusivity	κ	10^{-6}	m^2 s^{-1}	1
Critical Raleigh number	Ra_{cr}	1100		1
Gas constant	R	8.31	J K^{-1} mol^{-1}	2
Specific heat capacity, mantle	c	914	J K^{-1} kg^{-1}	1
Density, mantle	ρ_{mantle}	3400	kg m^{-3}	1
Density, crust	ρ_{crust}	2860	kg m^{-3}	3
Reference viscosity	ν_0	165	m^2 s^{-1}	1
Gravitational constant	G	6.67×10^{-11}	m^3 kg^{-1} s^{-2}	2
Core mass fraction	f_{core}	0.325		2
Earth radius	$R_\oplus$	6.372×10^6	m	2
Earth mass	$M_\oplus$	5.9742×10^{24}	kg	
Mantle temperature, initial	T_m ($t = 0$)	3273	K	
Temperature change causing e-folding in viscosity	T_ν	43 or 100	K	1 or 4

References. (1) Turcotte & Schubert 2002; (2) de Pater & Lissauer 2001; (3) Carlson & Herrick 1990; (4) Sleep 2007.

is the surface temperature, d is the depth to the CMB, g is the surface gravitational acceleration, α is the thermal expansivity, κ is the thermal diffusivity, ν is the viscosity, Ra_{cr} is the critical Raleigh number with value $\sim 10^3$, β is 0.3 (Schubert et al. 2001), A_0 is the activation temperature, and T_ν is the temperature increase (decrease) that decreases (increases) viscosity by a factor of e (Schubert et al. 2001). Equation (5) contains two equivalent parameterized expressions for T. Values used for these parameters are given in Table 2.

We neglect the pressure dependence of viscosity (Papuc & Davies 2008), which cannot be fully captured by parameterized models. In effect, we assume that the viscosity beneath the upper boundary layer, rather than some volume- or mass-averaged mantle viscosity, determines the properties of the flow.

We use the canonical values for H_i given by Turcotte & Schubert (2002), who estimate that 80% of Earth's current mantle heat flux is supplied by radioactive decay. Although Earth's surface heat flux is well constrained, the fraction of the flux out of the mantle that is due to radiogenic heat production is not. Literature values vary from $\leqslant 0.2$ (Lyubetskaya & Korenaga 2007) to 0.8 (Turcotte & Schubert 2002), with low values increasingly favored (Loyd et al. 2007). Variability in H_i could swamp any size signal in rates of volcanism, an important uncertainty addressed in Section 3.4. A useful rule of thumb is that a doubling a planet's concentration of radiogenic elements makes it behave like a planet with double the radius (Stevenson 2003).

Equations (3)–(5) can be solved directly for T. It is then easy to find the mass dependence of temperature (Section 3.1; Figure 2). However, secular cooling significantly contributes to the heat flux at the bottom of the lithosphere, so at a given time a planet will have a higher internal temperature and a higher heat flow than these thermal equilibrium calculations would suggest. Planets of different masses follow parallel cooling tracks (Stevenson 2003), and internal temperature is regulated by the dependence of mantle viscosity on temperature (Tozer 1970). A very simple model for mantle thermal evolution with temperature-dependent viscosity in plate tectonic mode is (Schubert et al. 2001)

$$\frac{\partial T}{\partial t} = \frac{H}{c} - k_1 (T_m - T_s)^{(1+\beta)} \exp\left(\frac{-\beta A_0}{T_m}\right), \quad (6)$$

where

$$k_1 = \frac{Ak}{cdM_{mantle}} \left(\frac{\alpha g d^3}{\kappa \nu_0 Ra_{cr}}\right) \quad (7)$$

and c is the specific heat capacity of the mantle rock.

We integrate this model forward in time from a hot start, using a fourth-order Runge–Kutta scheme. Because of the exponential temperature dependence of convective velocity, the transient associated with the initial conditions decays on a 100 Myr timescale, provided that the planet has a "hot start." Hot starts are overwhelmingly likely for differentiated massive rocky planets. Our initial condition is $T_m = 3273$ K, but our results are insensitive to increases in this value.

For planets in stagnant lid mode, we use the scaling of Grasset & Parmentier (1998)

$$T_c = T_m - 2.23 \frac{T_m^2}{A_o}, \quad (8)$$

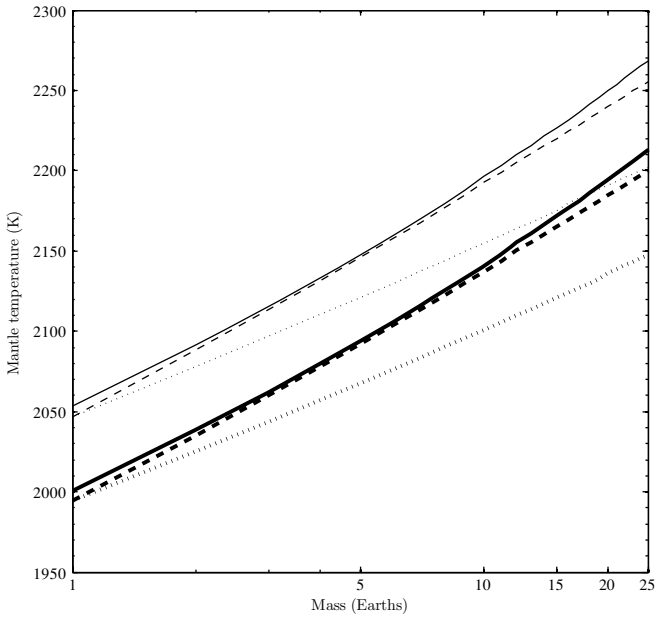

Figure 2. Effect of mass on mantle temperature for a planet in thermal equilibrium with a specific radiogenic power appropriate for today's Earth. Thick lines correspond to a surface temperature of 273 K, and thin lines correspond to a surface temperature of 647 K. The solid line uses the scaling of Seager et al. (2007), and the dashed lines use the scaling of Valencia et al. (2006): note that the latter is only valid for $M < 10$ Earths. The dotted lines use constant-density scaling. Seager et al. (2007) model cold exoplanets, leading to an underestimate of Earth's radius by 3%. The omission of thermal expansion leads to a smaller surface/area volume ratio than the other models, so the Seager et al. (2007) curves plot above those for Valencia et al. (2006) at low mass.

where T_c is the temperature at the base of the stagnant lid; plausible values lead to $(T_m - T_c) \ll T_m$. Then

$$Nu \approx \left(\frac{g\alpha(T_m - T_c)d^3}{\kappa\nu(T)Ra_{\rm cr}} \right)^{\beta}. \quad (9)$$

Since $T_c > T_s$, stagnant lid convection is less efficient at transporting heat than plate tectonics.

2.3. Melting Model

Earth generates 34 km^3 yr^{-1} of crust of which 63% is by isoentropic decompression melting at mid-ocean ridges (Best & Christiansen 2001). (This percentage understates the contribution of mid-ocean ridge melting to overall mantle degassing, because most of the volatile flux at arcs is just recycled from subducting crust.) After four decades of intensive study, this is also the best-understood melting process (Juteau & Maury 1999). Beneath mid-ocean ridges, the mantle undergoes corner flow. Melt is generated in a prism with triangular cross section, ascends buoyantly, and is focused to a narrow magma lens beneath the ridge. Petrological systematics require (Langmuir et al. 1992), and most melting models assume (Ghiorso et al. 2002), that the source magmas for mid-ocean ridge basalt melt fractionally or with small residual porosity, separate quickly, and suffer relatively little re-equilibration during ascent. For more massive planets, these remain robust assumptions. Buoyancy forces driving segregation are stronger and, because the pressure at which the solidus and adiabat intersect is at a shallower absolute depth, the ascent pathways are shorter. Because of these attractive simplifications and because mid-ocean ridge melting dominates Earth's crust production budget, we focus on mid-ocean ridge melting in this paper.

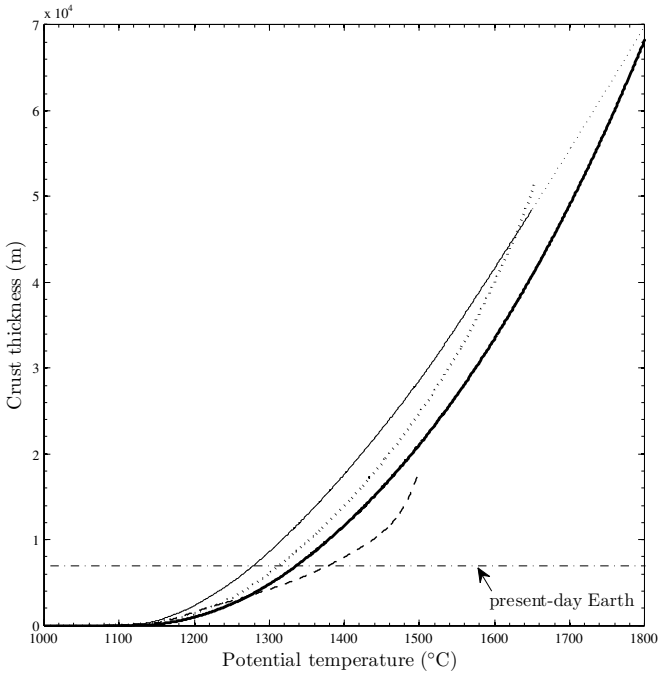

Figure 3. Crustal thickness as a function of potential temperature for $M_\oplus = 1$. Thick line corresponds to the model of Langmuir et al. (1992), which has a similar functional form to the models used by Sleep (2007) and Papuc & Davies (2008). Thin solid line corresponds to the MB88 model, thick dotted line to the K03 model, and dashed line to the pMELTS model. Thin dotted line is a cubic extrapolation of MB88 beyond its range of validity. pMELTS results are only shown where first melt occurs at <3 GPa. MB88 results are only shown where melt fraction is zero at 8 GPa. Horizontal dash-dotted line is observed crustal thickness on today's Earth.

Isoentropic decompression melting pathways are distinguished by their values of potential temperature, T_p. Actual temperatures of near-surface magmas are lower because of the latent heat of melting, the greater compressibility of melts with respect to solids, and, usually less important, near-surface conductive cooling. All mid-ocean-ridge melting schemes are very sensitive to T_p, especially just above the zero-pressure solidus. That is because increasing T_p both increases the pressure at which melting first occurs (lengthening the "melting column") and also increases the mass fraction of melting (X) suffered by the top of the melt column (Figure 1(c)). With the above assumptions,

$$P_{\rm crust} = -\int_{P_o}^{P_f} X(T, P)dP \quad (10)$$

$$T(P) = T(P + \delta P) - \left(\frac{\partial V}{\partial S}\right)\delta P + \left(\frac{\partial X}{\partial P}\right)L \quad (11)$$

$$T(P_o) = T_p + P_o\frac{\partial V}{\partial S}, \quad (12)$$

where $P_f = 0$ in the case of plate tectonics or $P_f = P_{\rm lith}$ (the pressure at the base of the lithosphere) in the case of stagnant lid convection; P_o is given by the intersection of the adiabat with the solidus, which is the point on the adiabat $\left(\frac{\partial V}{\partial S}\right)$ where $X = 0$, L is the latent heat of melting, and S is the entropy.

We use three models for $X(T, P)$. In order of increasing complexity, they are those of McKenzie (1984) as extended in McKenzie & Bickle (1988) (henceforth MB88), Katz et al. (2003) (henceforth K03), and (for plate tectonic models only)

Ghiorso et al. (2002), with the Smith & Asimow (2005) front-end (henceforth pMELTS). MB88 and K03 are similar in that they fit simple functional forms to experimental data, with MB88 more widely used although it is constrained by fewer data. pMELTS is a state-of-the-art model of phase equilibria for compositions similar to Earth's mantle. We use pMELTS throughout the predicted melting range, even though the model is only calibrated for use in the range 1–3 GPa. For pMELTS, we assume continuous melting with a residual porosity of 0.5% (that is, melt fractions greater than 0.5% are evacuated from the melting zone), and we use the mantle composition inferred to underly Earth's mid-ocean ridge system (Workman & Hart 2005) with 500 ppm water. Representative results with all these models are shown in Figure 3.

Each model is required to produce 7 km thick basaltic crust, which is the observed value on Earth (White et al. 2001), after 4.5 Gyr on an Earth-mass planet undergoing plate tectonics. We adjust the offset between potential temperature in the melting models, and the characteristic mantle temperature used in the thermal model, to obtain the observed crustal thickness. The required offset $T_m - T_p$ is 741 K, 707 K, and 642 K, for the MB88, K03, and pMELTS models, respectively (Figure 3).

3. MODEL OUTPUT

3.1. Simple Scaling Laws from Thermal Equilibrium Calculations

The simplest possible rocky planet model assumes that the ratio of radiogenic heat production to lithospheric heat flux (the convective Urey number), $Ur = 1$. We take the radiogenic-element concentrations given by Turcotte & Schubert (2002) (Table 1) and use Equations (3)–(5) to set mantle temperature. This is greater for more massive planets because their decreased surface area/volume ratio requires higher heat fluxes (and more vigorous convection) to dispose of the same heat flux. From Equations (3)–(5), but neglecting the dependence of Q on T_m,

$$\left(\frac{Ra}{Ra_\oplus}\right)^\beta = \left(\frac{M}{M_\oplus}\right)\left(\frac{A}{A_\oplus}\right)\left(\frac{d}{d_\oplus}\right) \quad (13)$$

which with $R \propto M^{0.25-0.28}$ (Valencia et al. 2006) gives $Ra \propto M^{\approx 2.45}$; using this simplification leads to a relation between temperature and mass

$$\nu(T) \propto M^{-5/4} \quad (14)$$

which when inserted into Equation (5) gives a good fit to the results shown in Figure 2. Similar scaling arguments with $R \propto M^{1/3}$ give $\nu(T) \propto M^{-8/9}$, i.e., an approximately straight line on a linear–log graph of temperature versus mass (Figure 2).

3.2. Plate Tectonics

We now turn to our time-dependent results.

1. *Thermal evolution.* As anticipated (Stevenson 2003), mantle temperatures for planets of different masses follow ~parallel cooling curves. Planets with $M = 2$ (5, 10, 25) $M_\oplus$ have potential temperatures 39 K (97 K, 146 K, 221 K) greater than Earth after 4.5 Gyr (Figure 4). There is little difference in thermal evolution between internal structure models: the temperature difference between Valencia et al. (2006) and Seager et al. (2007) is always <15 K (Figure 2). The constant-density planet runs significantly (up to 100 K) colder since it has a much larger surface area, but the same radiogenic-element complement. From now on we use only the thermal evolution calculations for the Seager et al. (2007) internal-structure model.
2. *Simple melting models, MB88 and K03.* Potential temperature increases monotonically with mass, so the pressure at the base of the crust also increases monotonically (Figure 3). However, the absolute thickness of the crust also scales as the inverse of gravity. In other words, although bigger planets run hotter, higher surface gravity moves the solidus and suppresses melting. For temperatures close to the solidus, the first effect dominates, and increasing planet mass increases crustal thickness (Figures 5(b) and (c)). Young and/or large planets show the opposite trend, with crustal thickness decreasing as planet mass increases. Crustal thicknesses are within a factor of 2 of each other for 1–25 $M_\oplus$ until 8.6 Gyr. After that, the ratio of crustal thicknesses diverges, as melting begins to shut down on the lowest-mass planets. In both models, for planets of intermediate mass and with ages slightly greater than the solar system, increasing mass has only a small (and negative) effect on crustal thickness. However, crust production per unit time increases with increasing mass, because more massive planets have more rapid plate spreading: see Section 5.1.
3. *pMELTS, a more complex melting model.* pMELTS predicts crustal thickness will increase rapidly with increasing planet mass for massive planets with ages comparable to the solar system (Figure 5(d)). Potential temperatures for these planets are >1500 °C. The predicted crustal-thickness result at these temperatures are suspect, because when $T_p > 1460$ °C, pMELTS predicts melting will occur to pressures greater than those for which it has been experimentally calibrated (<3 GPa). Crustal thickness is >1 km even after 13 Gyr in the pMELTs model, even for masses of 1 $M_\oplus$. This is because pMELTS-predicted crustal thickness ramps up slowly to 7 km crustal thickness

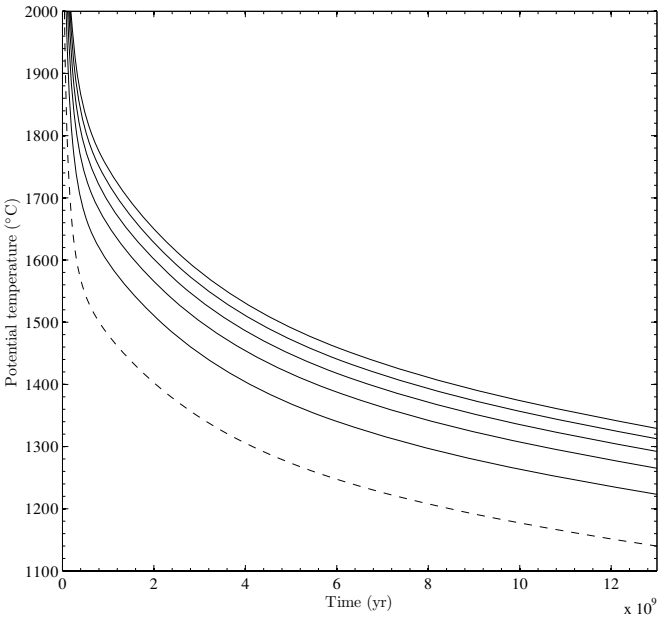

Figure 4. Effect of increasing planet mass on thermal evolution. Mantle temperatures are adjusted to produce 7 km thick crust with plate tectonics under MB88 melting model at 4.5 Gyr for 1 $M_\oplus$. Dashed line is 1 $M_\oplus$; solid lines are for 5, 10, 15, 20, and 25 $M_\oplus$, with temperature increasing with increasing mass. $T_\nu = 43$ K.

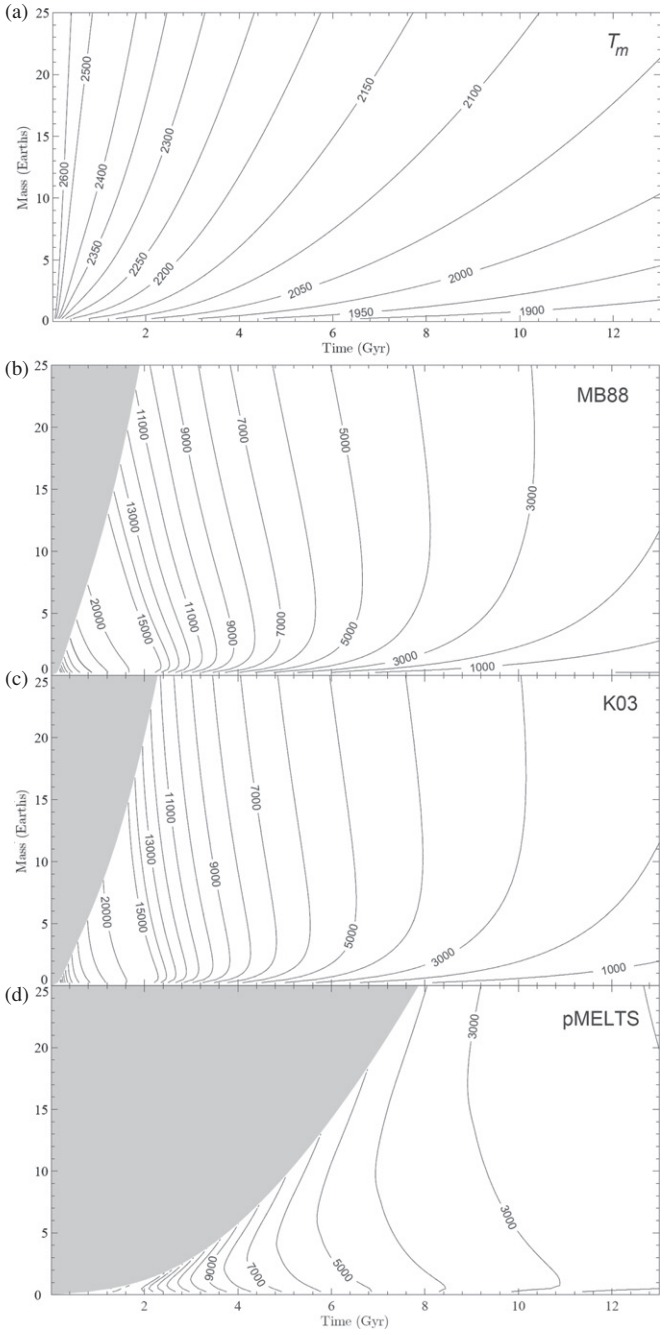

Figure 5. Uppermost panel: evolution of mantle temperature (°C) with time under plate tectonics. Seager et al. (2007) internal structure model. Initial temperature for all models is 3273 K. Lower panel, top to bottom: corresponding crustal thicknesses in meters for MB88, K03, and pMELTS melting modes. Contour interval is 1000 m from 0 to 15,000 m, and 5000 m for larger values. Light gray regions are where melting models are extrapolated beyond their stated range of validity. Horizontal line at bottom right of the MB88 pane corresponds to the cessation of volcanism on 0.25 $M_\oplus$ planets after ∼12 Gyr (see the text).

as temperature increases (Figure 3), so contours of constant crustal thickness are spaced more widely in temperature (equivalently, time) than with the other models. As with the other melting models, the planet mass that produces the thickest crust at a given time increases as the planets age.

To summarize, mass dependence increases with time as planets cool toward the solidus, and (for a given mass range) the sign of mass dependence changes with time. This is because of the strongly nonlinear behavior of melt production near the solidus; melting goes from zero to significant over a small range in potential temperature. Low-mass planets approach this temperature by 7–8 Gyr. Their crustal thickness declines more rapidly than on high-mass planets.

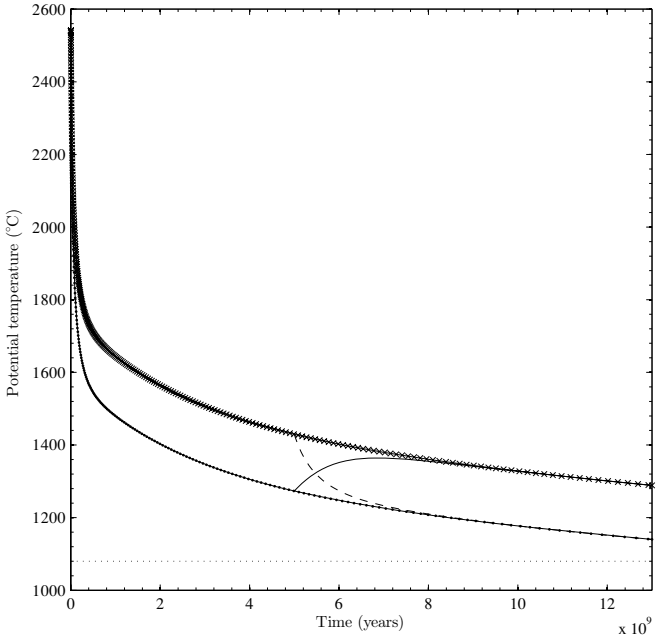

Figure 6. Effect of mode of mantle convection on thermal evolution. Stars joined by solid line correspond to stagnant lid mode. Dots joined by solid line correspond to plate tectonics mode. Thin solid line shows thermal evolution when an instantaneous switch to stagnant lid mode is imposed, after 5 Gyr, on a planet undergoing plate tectonics. The dotted line corresponds to the thermal evolution following an instantaneous switch to plate tectonics. For equivalent radiogenic complements, a planet in plate tectonics mode will have a lower potential temperature than a planet in stagnant lid mode. The difference is comparable to the range in potential temperatures due to mass.

3.3. Stagnant Lid

1. *Thermal evolution.* Because stagnant lid convection is less efficient at transferring heat than plate tectonics, a planet in which plate tectonics is suddenly halted will heat up (the thin solid line in Figure 6). This temperature rise reduces mantle viscosity, so Ra increases. Temperature converges on the evolutionary track of a planet that has always been in stagnant lid mode, with a characteristic convergence timescale of $(H\Delta T_{\rm mode})/cM_{\rm mantle} \sim 1$ Ga. A similar argument explains the temperature changes associated with going from stagnant lid mode to plate tectonics. The temperature difference between the tracks is $\Delta T_{\rm mode} \approx 160$ K for all masses. This is roughly $T_0\, ln\, ((T_m - T_s)/(T_m - T_c))$, which can be understood by equating the right-hand side of Equations (4) and (9). Therefore, the thermal evolution of stagnant lid planets follows Figure 5(a), but ≈160 K hotter.
2. *Stagnant lid melting.* Melt production within an ascending column of mantle in stagnant lid mode is truncated at the base of the lithosphere. For the same mantle temperatures, predicted erupted thickness is much smaller (Equation (10)). This effect opposes the increased temperature of stagnant-lid mantles. To produce Figure 7 we use the same mantle-potential temperature offsets as in plate tectonic mode (so the model is still "tuned to Earth"). Most planets run hotter in stagnant-lid mode to the extent that pMELTS cannot be used, as T_p exceeds the range over

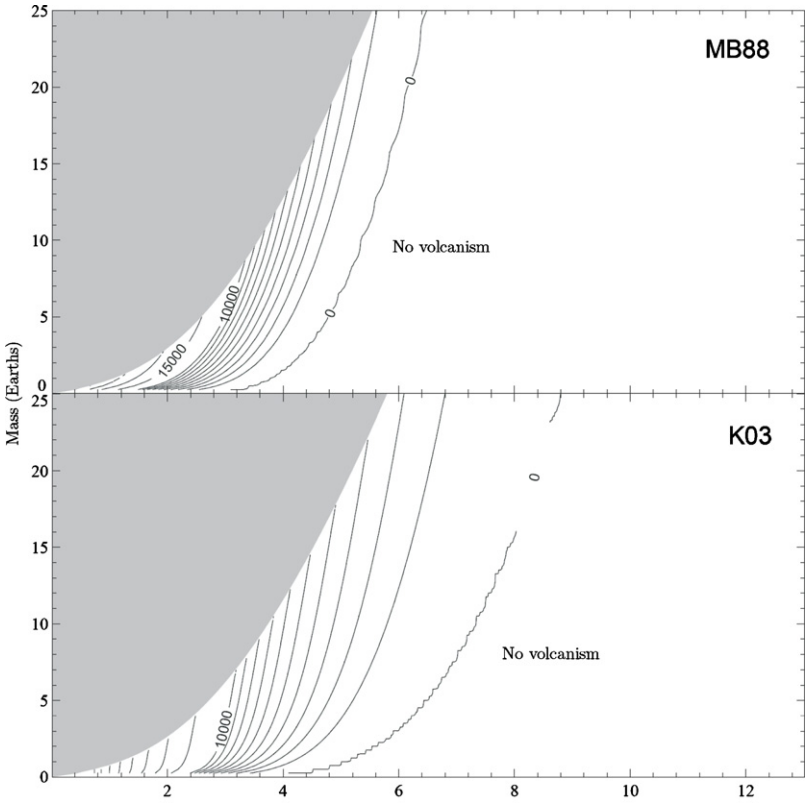

Figure 7. Evolution of crustal thickness with time in stagnant lid mode, for MB88 (top) and K03 (bottom) melting models. Wiggles in the CT = 0 contour are interpolation artifacts.

which it is calibrated. The MB88 and K03 models show roughly the same behavior in stagnant lid mode (Figure 7). For young (<2–3 Gyr) planets, an ascending column of mantle produces more melt in a stagnant lid mode than in plate tectonic mode—the higher temperature matters more than the (small) lithospheric thickness. For somewhat older planets, an ascending column of mantle produces less melt in stagnant lid mode than in plate tectonic mode. The temperature difference is much the same, but the growing lithosphere increasingly truncates the melting column. At a mass-dependent age much less than the age of the Galaxy, melting ceases.

3. *What controls cessation of melting?* For a given melt production function, all planets in plate tectonics mode will cease volcanism at the same potential temperature. Consequently, a planet's volcanic lifetime is delineated by an isotherm (T_p = 1080–1193 °C, depending on the melting model). For planets in stagnant lid mode, this is not the case. There is still a one-to-one relationship between temperature and the absolute thickness of the lithosphere. However, the absolute thickness of the melt zone at fixed temperature decreases with increasing gravity, but $z_{\rm lith}$ does not. Thus, $z_{\rm lith}$ increasingly truncates the melt zone as gravity increases. As a result, there is a temperature range for which low-mass planets can sustain melting in stagnant lid mode, whereas high–mass planets cannot. Over the mass range 1–25 $M_\oplus$, this temperature range is ∼180 K. Consequently, in stagnant lid mode, more massive planets run much hotter but cease melting only moderately later than smaller planets (Figure 7).

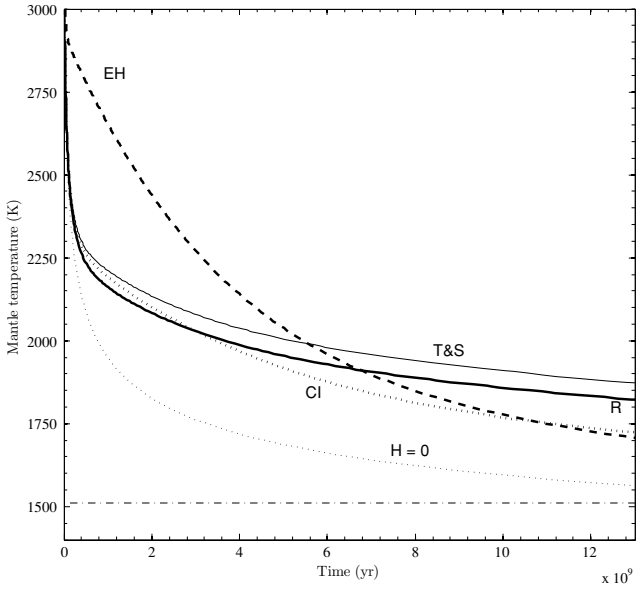

Figure 8. Effect of different radiogenic-element complements on thermal evolution. Initial mantle temperatures are identical; all runs are with $T_v = 43$ K. Thick lines correspond to various chondritic scenarios: thick dashed line is EH chondrite; thick dotted line: CI chondrite; thick solid line: Ringwood (1991). The thin solid line is for Turcotte & Schubert (2002), and the thin dotted line is for no radiogenic elements in the mantle. This could correspond, for example, to early and complete differentiation of the mantle to produce a thick crust, which is then swiftly removed by impacts. The horizontal dash-dotted line at 1510 K corresponds to $Nu = 1$ (no convection, no large-scale mantle flow, and no potential for sustained melt production).

3.4. Initial Bulk-Chemistry and Initial Radiogenic-Power Variations

"Noncanonical" initial radiogenic-element complements have been suggested for Earth. To evaluate this possibility, we show 1 $M_\oplus$ thermal evolution tracks with radioisotope complements appropriate to "undepleted" mantle (Ringwood 1991), CI chondrites (Anders & Grevesse 1989), and EH chondrites (Newsom 1995) (Table 1; Figure 8). The CI and "undepleted" tracks show similar behavior to T&S, but the U^{235}-rich, U^{238}-poor EH chondrite track shows more rapid cooling. Since we use Earth's observed oceanic crust thickness to tune mantle temperature, it is not particularly important to get the absolute values right, and three of the four radiogenic-element complements tested have similar behavior over geological time.

The long-term thermal evolution of rocky planets depends on the abundance of the long-lived radioisotopes ^{232}Th, ^{235}U, and ^{238}U at the time of planet formation. These are produced only by the rapid neutron capture process (*r*-process) acting on the iron-peak isotopes. This is thought to occur only during explosive nucleosynthesis in stars with 10–20 $M_\odot$ (Chen et al. 2006). In contrast, Si is produced during α-chain process by the whole range of massive stars. Th, and especially U, are difficult to detect in stars but europium (Eu), another exclusively *r*-process element, can be readily measured. The average observed stellar abundance of Eu to silicon decreases by a factor of 0.63 as the abundance of heavy elements or metallicity (represented by iron Fe) increases by a factor of 100 to the solar value (Cescutti 2008). The *r*-process appears to be universal and all *r*-process elements scale closely with solar values (Frebel 2008). Therefore, the average abundance of ^{232}Th, ^{235}U, and ^{238}U isotopes can be predicted using the trend of Eu with abundance or metallicity, the age–metallicity relationship of the Galaxy, the star formation history of the Galaxy, and the half-life of each isotope. We adopt a simple linear age–metallicity relationship with an increase of 1 dex (a factor of 2.5) over the age of the Galaxy, with solar metallicity occurring 4.6 Gyr ago (e.g., Pont & Eyer 2004). Figure 9 plots the predicted abundance of the three isotopes using the observed trend of Eu and the Prantzos & Silk (1998) parameterization of the star formation history of the Galaxy. (The predictions are only weakly sensitive to the model of star formation.) The age of the Galaxy is taken to be 13.6 Gyr. All abundances are normalized to the value at the formation of the Sun.

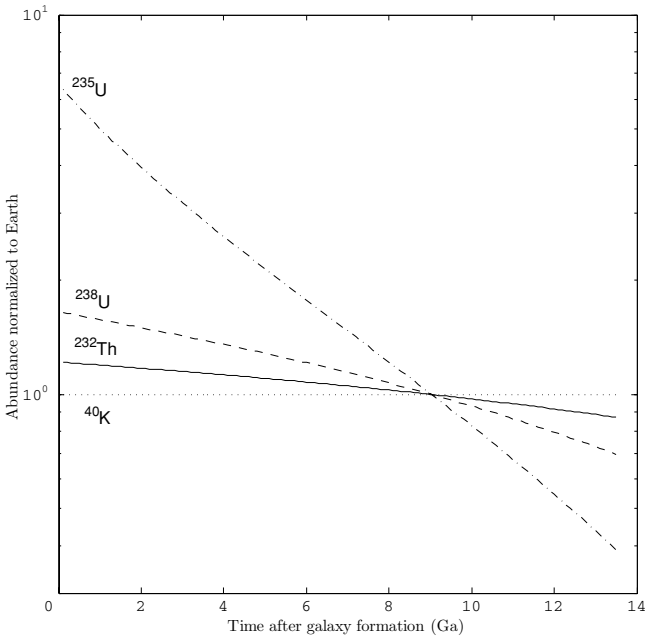

Figure 9. Abundance, relative to silicon and normalized to conditions at the time of the protosolar nebula, of the principal long-lived radionuclides in rocky planet mantles.

Planets forming early in the history of the Galaxy would have 50% more ^{238}U, but six times more ^{235}U, than Earth. The higher abundance is because the amount of radioisotopes in the interstellar medium only reflects massive star formation over a few half-lives, whereas ^{28}Si and other stable isotopes accumulate over the history of the Galaxy. Therefore, these systems are not U- and Th-rich, they are Si-poor. The high abundance of ^{235}U could have an important role in the *early* thermal history of such planets.

The effect of these trends on *present-day* planets, while still significant, is more modest simply because they are older. Figure 10 plots planet mantle temperature against the age of the

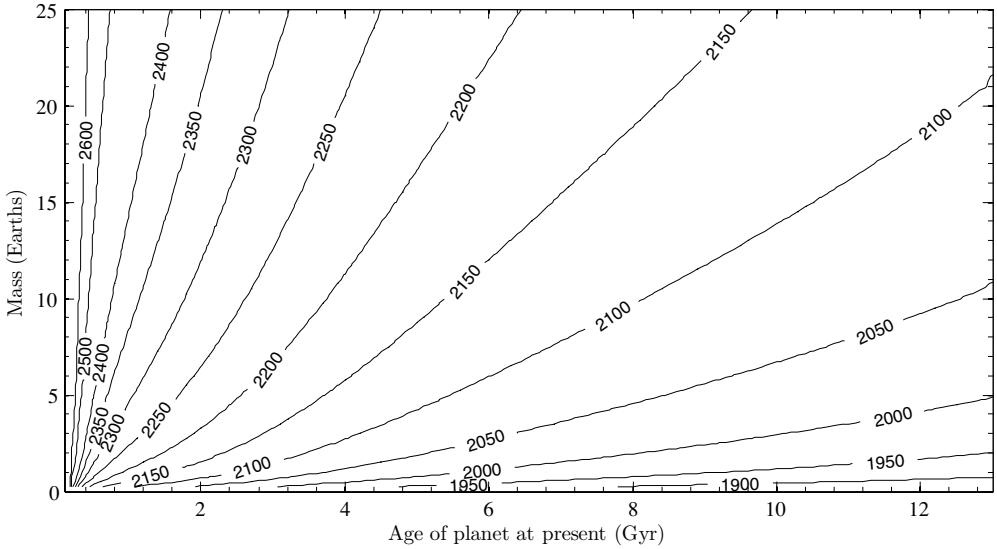

Figure 10. Temperature at the present epoch, tracking the effect of galactic cosmochemical evolution on initial radioisotope complement. Planets plotting to the left orbit young stars, and planets plotting to the right orbit old stars. Compare with the top panel of Figure 10. Note that the abscissa is not time, but the age of planet at the present day.

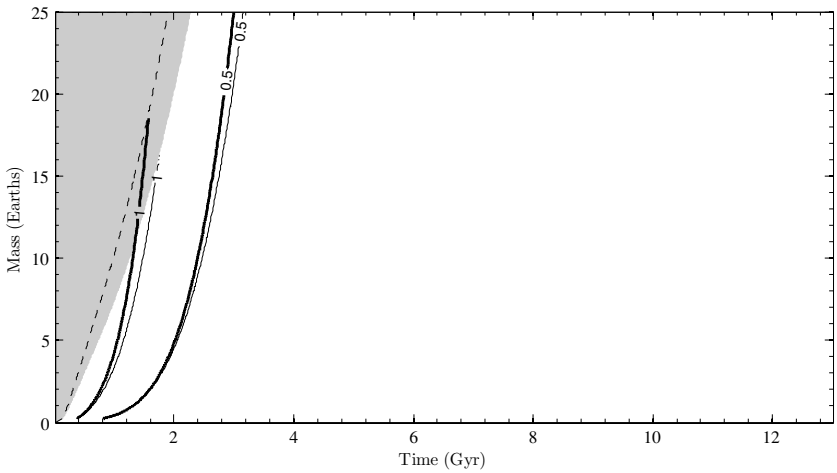

Figure 11. Possible limits to plate tectonics. Thick solid lines correspond to crust-to-lithosphere thickness ratios of 0.5 and 1.0 for the MB88 melting model; thin solid lines are the same, but for the K03 melting model. Points to the left of these solid lines may be subject to vertical (Io-type) tectonics. Dotted line is the limit of validity of the MB88 melting model. Results not shown for the pMELTS melting model because solid lines fall in the temperature region for which pMELTS is not valid.

host star. Comparison with Figure 5(a) shows that inclusion of cosmochemical trends in H_i lowers T_m by up to 50 K for young planets, while raising T_m by up to 40 K for old stars, compared to their present-day temperature had they formed with an Earth-like inventory of radiogenic elements.

We have assumed that the major-element composition of planetary mantles is similar everywhere and at all times. This is unlikely to be true in detail: for example, it has been proposed that on early Earth the mid-ocean ridge basalt source was more depleted than at the present day (Davies 2007). Earth's continent mass fraction may be higher (Rosing 2006), or lower than is typical. More severe variations in major-element composition, with correspondingly major shifts in rheology and in the solidus, can be imagined (e.g., Gaidos 2000; Kuchner & Seager 2005). Even highly oxidized "coreless" planets have been modeled (Elkins-Tanton & Seager 2008b). We leave the geodynamic consequences of such variations as an open subject: a future objective will be to use geodynamic observables to constrain internal structure and bulk composition.

4. EFFECT OF MELTING ON THE STYLE OF MANTLE CONVECTION

We have shown that transitions between plate tectonics and stagnant lid mode have an impact on thermal evolution comparable to that of mass over the range of masses considered in this paper. With this motivation, we now assess whether plate tectonics is viable on more massive Earth-like planets. Our approach will be to use our comparatively robust understanding of melting to examine conditions under which other forms of heat transfer supplant Earth-like plate tectonics. Vertical tectonics, as seen on Io (Moore 2003; Lopes & Spencer 2007) may be thought to take over from horizontal (plate) tectonics when either (1) the thickness of the crust becomes comparable to that of the lithosphere, (2) heat lost by magma transport dominates over conduction, or (3) the crust delaminates. We also assess the likelihood that (4) continental growth or (5) greater plate buoyancy prevents subduction. We present results only for our fiducial calculation with MB88 melting and radiogenic-isotope complements following Turcotte & Schubert (2002).

We assume throughout that surface water is available to hydrate lithosphere rock. Weakening the lithosphere by hydration is thought to be a prerequisite for plate tectonics.

4.1. Crust Thicker Than Lithosphere

If the crustal thickness $Z_{\rm crust}$ is comparable to the lithospheric thickness $Z_{\rm lith}$, the lower crust is likely to melt and form buoyant diapirs. Widespread intracrustal diapirism within the oceanic crust is not known on Earth and, if it were a major heat sink for the mantle, would be a substitute for plate tectonics. $Z_{\rm lith}$ scales as Q^{-1}, and on Earth the equilibrium value of $Z_{\rm lith}$ is $\sim$110 km (McKenzie et al. 2005). Therefore,

$$\left(\frac{Z_{\rm crust}}{Z_{\rm lith}}\right) = \frac{7}{110}\left(\frac{Q}{Q_{\rm Earth}}\right)\left(\frac{Z_{\rm crust}}{Z_{\rm crust,Earth}}\right). \quad (15)$$

We find $Z_{\rm crust}/Z_{\rm lith} < 1$ for all planets >2 Gya (Figure 11), so intracrustal diapirism is unlikely within equilibrium lithosphere. Intracrustal diapirism is unlikely to be the limiting factor for super-Earth plate tectonics.

4.2. Magma Pipe Transport Energetically Trumps Conduction

On Earth, heat lost by conduction through thin lithosphere near mid-ocean ridges greatly exceeds heat lost by advection of magma. On Io, the opposite is true: most internally deposited heat is lost by advection of magma through lithosphere-crossing magma conduits—"magma pipes" (Moore 2001). Such a planet, although it may have limited plate spreading, is not in plate tectonic mode; vertical rather than horizontal motion of the material making up the lid is the more important process.

We introduce the dimensionless "Moore number," Mo, in appreciation of the work of Moore (2001, 2003), which we define to be the ratio of magma pipe heat transport, $Q_{\rm magma}$, to heat lost by conduction across the lithosphere, $Q_{\rm cond}$. To calculate how this number (analogous to a Peclet number) scales with increased mass, we specify that total heat loss (magma pipe transport plus conduction across the boundary layer) adjusts to match the heat loss across the boundary layer prescribed by the thermal evolution model:

$$Mo = \frac{Q_{\rm magma}}{Q_{\rm cond}} = \frac{Q}{Q_{\rm cond}} - 1. \quad (16)$$

An upper bound on magma pipe transport is to assume that all melt crystallizes completely and cools to the surface temperature. In that case

$$Q_{\rm magma} = \rho_{\rm crust}(c_b \Delta T_1 + E_{\rm lc}) Z_{\rm crust} l_r s \sim c_1 s, \quad (17)$$

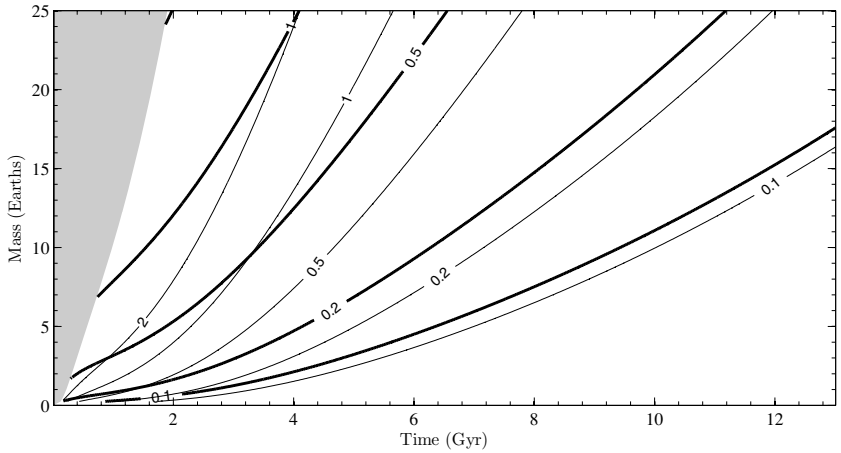

Figure 12. Plate spreading rate (m yr^{-1}) as a function of time. Thick lines correspond to solution including heat transport through magma pipes. Thin lines correspond to conduction-only solution. MB88 melting model.

where $\rho_{\rm crust}$ is the crustal density, c_b is the specific heat of basalt, ΔT_1 is the temperature contrast between lava and the surface, $E_{\rm lc}$ is the latent heat of crystallization, l_r is the ridge length, and s is the spreading rate. Provided that half-space cooling is a good approximation to the thermal evolution of plates,

$$Q_{\rm cond} = 2k\Delta T_2 \left(\sqrt{\frac{A_{\rm oc} l_r}{\pi\kappa}}\right)\sqrt{s} \sim c_2\sqrt{s}, \qquad (18)$$

where $A_{\rm oc}$ is the area of the ocean basins only, which we take to be $0.6 \times A$ as on Earth. We can now solve the quadratic in s

$$Q^2 = c_1^2 s^2 + c_2^2 s. \qquad (19)$$

Finally, we obtain an expression for Mo:

$$Mo = \frac{Q_{\rm magma}}{Q_{\rm cond}} = \left(\frac{\rho_{\rm crust}(c_b\Delta T_1 + E_{\rm lc})Z_{\rm crust} l_r}{2k\Delta T_2\sqrt{Al_r}/(\sqrt{\pi\kappa})}\right)\sqrt{s}. \qquad (20)$$

Here, l_r is the ridge length and s is the spreading rate. We assume a latent heat of crystallization $E_{\rm lc} = 550$ kJ kg^{-1}, a specific heat of basalt $c_b = 0.84$ kJ kg^{-1} K^{-1}, crustal density $\rho_{\rm crust}$ of 2860 kg m^{-3} (Carlson & Herrick 1990), base lithosphere temperature of 1300 °C, and lava temperature of 1100 °C and surface temperature of 0 °C giving $\Delta T_1 = 1100$ K and $\Delta T_2 = 1300$ K. This gives 4.2×10^{18} J in melt km^{-3} plate made. As an illustration, for Earth (mid-ocean ridge crust production 21 km^3 yr^{-1}), $Q_{\rm magma}$ is 2.8 TW. The total oceanic heat flux is 32 TW, so today's Earth has a $Mo \sim 0.10$.

Therefore, given the one-to-one relationship between Q and T_p, we can solve for spreading rate (Figure 12). As $Mo \to 0$, $s \to Q^2$ (Sleep & Zahnle 2001). Note that the characteristic age at subduction $\tau = A/(2l_r s)$. As a consequence, the Moore number does not vary with different possible scalings of ridge length (equivalently, plate size) with increased planet mass. As planet mass increases, we hold plate area (rather than the number of plates) constant to produce Figure 12. If one instead holds the number of plates constant, l_r falls and s increases, but, because τ is unchanged, our subsequent buoyancy and rate of volcanism calculations (Sections 4.4 and 5) are not affected. For Earth, Equation (18) gives $s \sim 5$ cm yr^{-1}, a good match to present-day observations (minimum <1 cm yr^{-1} in the Arctic Ocean, maximum 15 cm yr^{-1} at the East Pacific Rise, mean $s \sim$ 4 cm yr^{-1}).

Reaching $Mo \sim 1$ requires temperatures near or beyond the limit of validity of our melting models. Coincidentally, $Mo = 1$ plots close to $Z_{\rm crust}/Z_{\rm lith} = 1$ on a mass–time graph. We conclude that heat-pipe cooling is not dominant for Earth-like planets >2 Gyr old.

4.3. Phase Transitions Within Crust

Basalt, which is less dense than mantle rock, undergoes a high-pressure exothermic phase transition to eclogite, which is more dense than mantle rock (Bucher & Frey 2002). Except during subduction, the pressures at the base of Earth's basaltic crust are too low to make eclogite. However, the pressures at the base of the crust on massive Earth-like planets are far greater. If the crust of a massive Earth-like planet includes an eclogite layer at its base, this may delaminate and founder, being refreshed by hotter mantle (Vlaar et al. 1994).

We tracked temperature and pressure at the base of the crust for planets in plate tectonics mode, and compared these with the phase boundaries for eclogite plotted in Figure 9.9 of Bucher & Frey (2002). We assumed uniform thermal conductivity within the thermal boundary layer. We found that eclogite is not stable for $M < 25\ M_\oplus$. As planet mass increases, the ratio of crustal to lithospheric thickness increases, while mantle temperature also rises. Consequently, the temperature at the base of the crust rises, inhibiting the exothermic eclogite-forming reaction.

4.4. A Continental Throttle?

Continental crust may sequester radiogenic elements, inhibiting plate tectonics and melting by imposing more rapid mantle cooling. The limit is a fully differentiated planet, in which successive melting events have distilled nearly all radiogenic elements into a thin shell near the surface. Independent of this effect, too great an area of nonsubductible, insulating continents may itself be enough to choke off plate tectonics—a limit of 50% of total area has been suggested (Lenardic et al. 2005). Which limit is more restrictive to plate tectonics? On Earth, continents contain 26%–77% of the radiogenic complement of Bulk Silicate Earth (Korenaga 2008), and cover ~40% of the planet's surface area. If the threshold value for a significant nonsubductible-cover effect on mantle dynamics is 50% (Lenardic et al. 2005), this limit will be passed before complete differentiation occurs. However, all radiogenic elements would be sequestered in continental crust before continental coverage

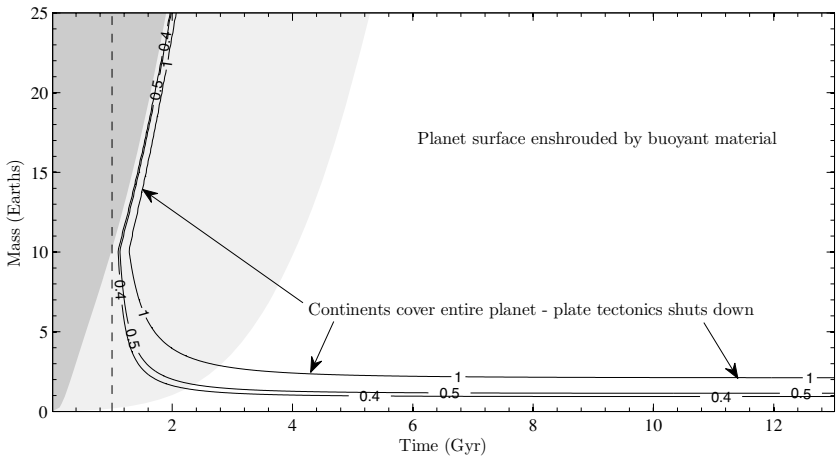

Figure 13. Fractional area covered by continents vs. time. MB88 melting model. The dark shaded region is that for which the melting model is invalid. The light shaded region is that for which buoyancy stresses probably prevent plate tectonics. The vertical dashed line is the time after which continental growth is permitted (1 Gyr; Condie & Pease 2008). For $M_{\oplus} > 10$, continents choke plate tectonics $\leqslant$0.3 Gyr after continent growth is permitted.

reached 100%. We expect that the thickness contrast between continental and oceanic crust will scale as the inverse of gravity. This is because crustal thickness variations are limited by crustal flow (and brittle failure down gravitational-potential-energy gradients). If in addition the radiogenic-element content of continental crust does not vary, then we can relate the two limits by expressing the fraction of planet surface area covered by continents as

$$f_{\rm area} = \frac{V_{\rm cont}}{A Z_{\rm crust}} \propto \frac{f_{\rm radio} M}{M^{1/2} M^{-1/2}} \propto f_{\rm radio} M, \qquad (21)$$

using the approximation $R \propto M^{\sim 0.25}$. This implies that continental coverage will be the more severe limit for massive planets as well. A massive planet will enshroud itself with nonsubductible crust before it sequesters a substantial fraction of its radiogenic elements into crust.

Provided that crustal flow limits continental thickness, a representative calculation shows that continents will spread out to coat the surface of an Earth-like planet $>3\ M_{\oplus}$ in much less than the age of the Earth (Figure 13); this is because continental production rate scales roughly as planet mass, but planet area increases only as the square root of mass. To produce this figure, we set net continental growth to zero for the first 1 Gyr of each planet's evolution (guided by the age of the oldest surviving continental blocks on Earth). From 1 Gyr forward, we set continental growth to be proportional to crustal production rate, with a proportionality constant picked to obtain 40% coverage on Earth today.

4.5. Will Trenches Jam?

Subduction will cease if the relative buoyancy of crust, less dense than mantle, exceeds that of the colder and denser lithospheric mantle. Provided that thermal conductivity and crustal density are constant, the subduction condition is

$$\Delta\rho \cong -\rho_{\rm lith} + \frac{1}{Z_{\rm lith}}(\rho_{\rm lith}(1+\alpha\Delta T_3)(Z_{\rm lith} - Z_{\rm crust}) + (\rho_{\rm crust} Z_{\rm crust})) < 0, \qquad (22)$$

where

$$\Delta T_3 = \frac{1}{2}\left(1 - \frac{Z_{\rm crust}}{Z_{\rm lith}}\right)\Delta T_2 \qquad (23)$$

and $\Delta\rho$ is the density difference favoring subduction, $\rho_{\rm lith}$ is the reference density of mantle underlying the plate, $Z_{\rm lith}$ is the lithospheric thickness, ΔT_3 is the average cooling of mantle lithosphere, all evaluated at subduction.

Hotter—that is, bigger or younger—planets must recycle plate faster, so a plate has less time to cool. In addition, higher potential temperatures produce a thicker crust. Both factors tend to produce positively buoyant plate, which is harder to subduct. This effect is more severe for massive planets because of their greater gravity.

Once subduction is initiated the basalt-to-eclogite transition can sustain subduction. However, it is not clear that subduction initiation is possible if plate is positively buoyant everywhere, as seems likely for early Earth (Davies 1992; Sleep 2000). The geological record is neither mute nor decisive. All but the last Gyr of Earth's tectonic history is disputed, but evidence is accumulating that subduction first occurred at least 2.7 Gya (1.8 Ga after formation), and perhaps earlier than 3.2 Gya (1.3 Ga after formation; Condie & Pease 2008). Taking buoyancy stress per unit length of trench to be the appropriate metric for buoyancy, we can relate Archean observations to high-mass planets (Figure 14). For example, the buoyancy stress that had to be overcome on Earth after 1.8 Ga is the same as that on a 16 $M_{\oplus}$ planet after 4.5 Ga. Here we have assumed that all plate reaches the subduction zone at a characteristic age, τ, that the temperature distribution within the plate is described by half-space cooling (so $Z_{\rm lith} = 2.32\,\kappa^{0.5}\tau^{0.5}$), and that k and $\rho_{\rm crust}$ (2860 kg m^{-3}; Carlson & Herrick 1990) are constant. This gives a negative (subduction-favoring) buoyancy stress of 38 MPa at the characteristic age of subduction on the present Earth. The much more sophisticated model of Afonso et al. (2007) yields 21 MPa, so our estimate probably understates forces retarding subduction. However, the base of a thick, water-rich crust may be at temperatures/pressures permitting amphibolite-grade metamorphism, producing dense crust. (In addition, the crust-mantle density contrast declines with increasing melt fraction as the olivine content of the crust increases). For this reason, we also plot results for a constant crustal density of 3000 kg m^{-3}, intermediate between the densities of amphibolite (3000–3300 kg m^{-3}; Cloos 1993) and unmetamorphosed crust. Whether or not amphibolitization is considered, our assessment is that plate buoyancy raises a severe

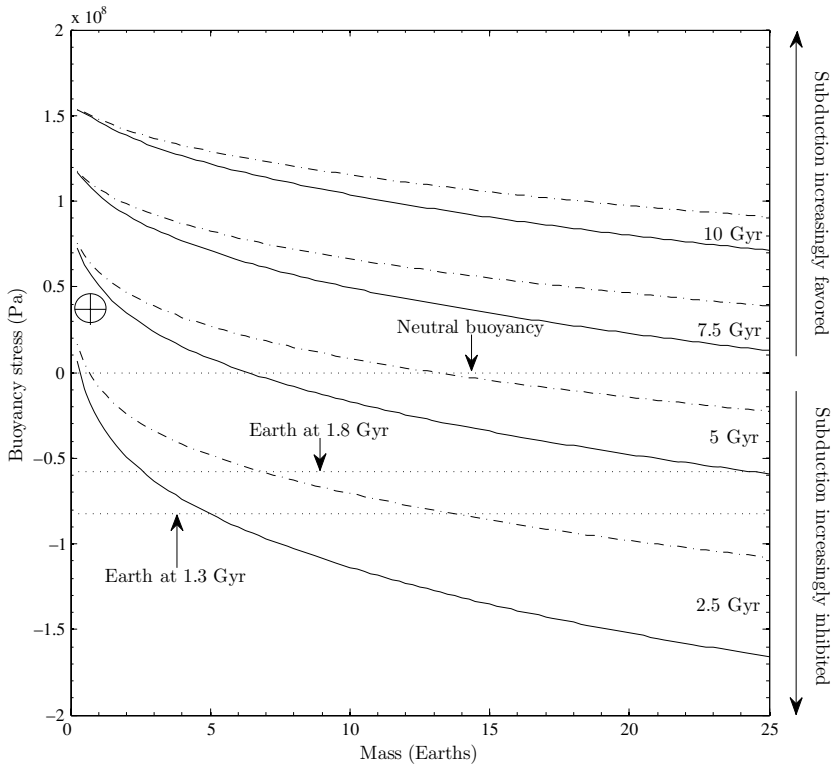

Figure 14. Buoyancy stresses as a function of thermal evolution and planet mass. Buoyancy stress is the product of density contrast, gravity, and lithospheric thickness. Positive values denote plate denser than underlying mantle, favoring subduction; negative values denote plate more dense than underlying mantle, retarding subduction. Solid lines connect buoyancy values for planets of different masses 2.5 Gyr, 5 Gyr, 7.5 Gyr, and 10 Gyr after planet formation, for constant crustal density of 2860 kg m^{-3}. Dash-dotted lines are for a crustal density of 3000 kg m^{-3}, as might be the case for partial amphibolitization. Dotted lines are possible lower limits to plate tectonics based on Earth's (disputed) geological record; arguably, subduction must be possible on planets whose buoyancy forces plot above these lines. The Earth symbol is the model calculation for present-day conditions on Earth.

hurdle for plate tectonics on massive Earths, and may well be limiting.

5. RATE OF VOLCANISM AND IMPLICATIONS FOR DEGASSING

5.1. Degassing Rate

In plate tectonics mode, for "Earth-like" planets with oceans and some land, we calculate the rate of volcanism by multiplying spreading rate (Section 4.3), mid-ocean ridge length, crustal thickness (Section 3), and crustal density, then dividing by planet mass (Figure 15). Our model gives 1.2×10^{-11} yr^{-1} by mass for Earth, observations give 1.1×10^{-11} yr^{-1} (Best & Christiansen 2001). The discrepancy is mainly due to our model's higher-than-observed spreading rate (Section 4.3). For comparison, Earth's total observed present-day rate of volcanism is 1.7×10^{-11} yr^{-1} by mass, and 3.1×10^{-11} yr^{-1} by volume (Best & Christiansen 2001). This includes arc and ocean-island volcanoes, which are not modeled in this paper. Rate per unit mass increases monotonically with increasing mass, for all times. Per unit mass, rates of volcanism vary only by a factor of 3 on planets <3 Gyr old and >1 $M_\oplus$, but a stronger mass dependence develops for older planets (Figure 15). Melting in plate tectonic mode ceases when potential temperature falls below the zero-pressure solidus, but this only occurs for small (0.25 $M_\oplus$) planets $\geqslant$ 10 Gya (Figure 5(b)).

In plate tectonic mode, the flux of mantle into the melting zone balances spreading rate. To calculate the rate of volcanism on a planet in stagnant lid mode (Figure 16), we must first find the flux of material into the upper boundary layer as a function of Ra. We define a near-surface convective velocity such that all heat flow in excess of the conductive heat flow is advected

$$Nu - 1 = \frac{u\Delta T_{\rm conv}\rho c}{2\left(\frac{k\Delta T_{\rm cond}}{d}\right)} = \frac{u\rho c d}{2k}\left(\frac{T_m - T_c}{T_m - T_s}\right)$$

$$u = 2(Nu - 1)\left(\frac{k}{\rho c d}\right)\left(\frac{T_m - T_s}{T_m - T_c}\right), \quad (24)$$

where the factor of 2 takes account of the need for downwelling material to balance upwelling. The crust production mass flux, normalized to planet mass, is

$$R = \frac{Au\rho}{M_{\rm planet}}\left(\frac{\rho_{\rm crust} Z_{\rm crust} g}{P_f - P_o}\right), \quad (25)$$

where R is the rate of melt generation per unit mass, $Z_{\rm crust}$ is obtained from our models in Section 3, and the bracketed term is the mean melt fraction. This sets an upper limit to the rate of volcanism (Figure 16) because it assumes that all melt generated reaches the surface, and that all ascending mantle parcels reach P_o. The first assumption is probably safe because of the large forces driving magma ascent on massive planets, and the short absolute distances they must ascend. With these assumptions, we find that the rate of volcanism on stagnant lid planets initially exceeds that on their plate tectonic counterparts but this contrast soon reverses as the stagnant lid thickens. The predicted shutdown of nonplume melting on stagnant lid planets shows remarkably weak dependency on mass and melting model, as explained in Section 3.3. We consider the rate of crust production

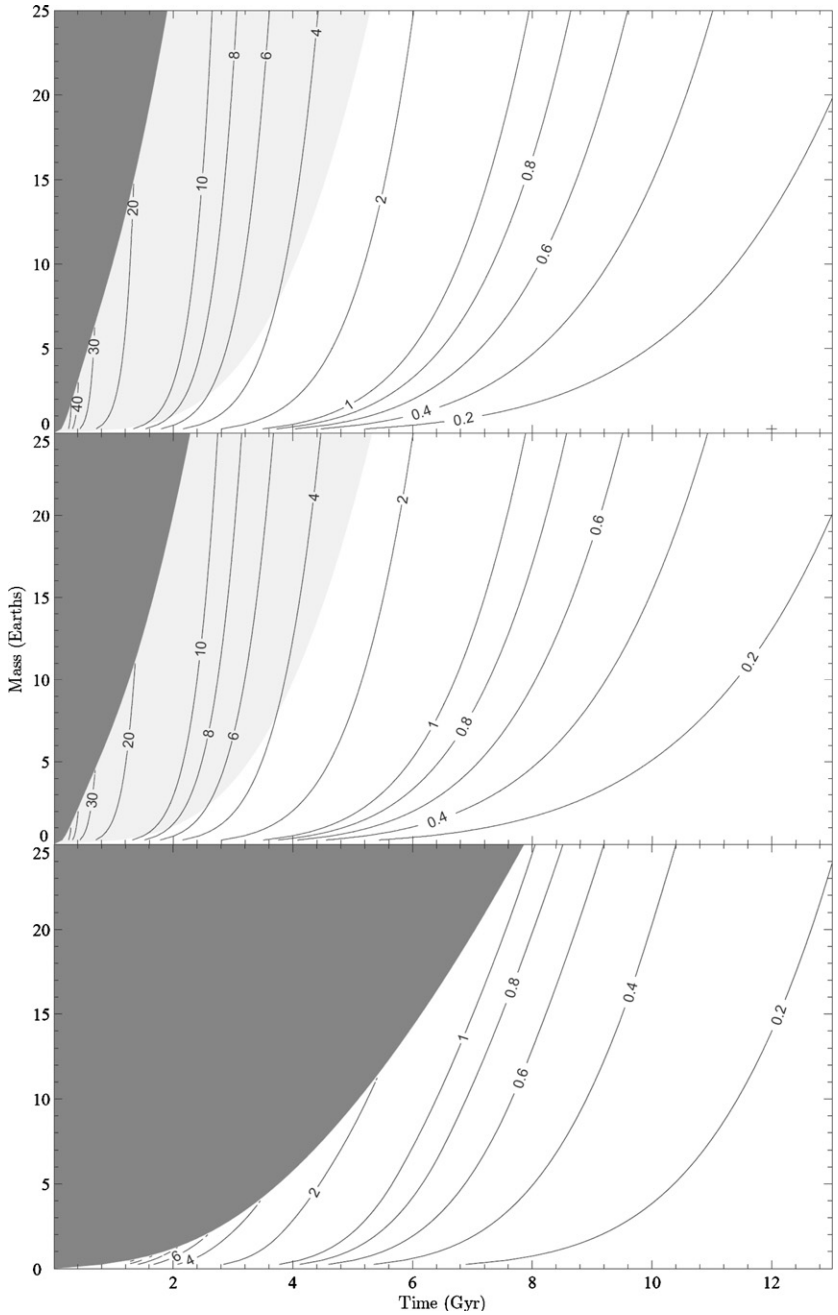

Figure 15. Rate of volcanism per unit mass on massive Earth-like planets experiencing plate tectonics, normalized to calculated rate on the Earth (3.7516×10^{-19} s^{-1}, equivalent to 24 km^3 yr^{-1}), for MB88 (top), K03 (middle), and pMELTS (bottom) melting models. Light gray shaded regions correspond to negative buoyancy stresses with magnitudes in excess of 50 MPa, which would markedly inhibit subduction. Dark gray shaded regions correspond to mantle temperatures too high for a reliable crustal thickness calculation.

to be a good proxy for the rate of degassing. But because volatiles are incompatible, they partition almost quantitatively into even small fractions of melt. Therefore, a more accurate statement is that degassing should be proportional to the flux of mantle processed through melting zones (Papuc & Davies 2008). We had great difficulty in determining this processing flux because of the "solidus rollover" problem (Section 6.2). (Because of volatile incompatibility, order-unity differences in the volatile concentrations of planetary mantles should not make much of a difference to our melting curves. Wet parcels of ascending mantle soon "dry out.") In addition to lavas that are extruded at the surface, magmas that crystallize below the surface as intrusions—such as the sheeted dykes and gabbros of Earth's oceanic crust—are assumed to degas fully and are referred to as "volcanism."

The implications for greenhouse-gas release of our results depend on the water and CO_2 contents of extrasolar planet mantles. These will depend on the mantle's oxidation state (Elkins-Tanton & Seager 2008b), the range of semimajor axes from which the growing planet draws material, and the extent of volatile loss on the planetesimals which collide to form the planet. The water and CO_2 contents of terrestrial magmas are our only empirical guide. At mid-ocean ridges, these range from 0.1%–1.5% for H_2O, and 50–400 ppm for CO_2 (Oppenheimer 2003). Taking the upper-limit values (which is appropriate, given that additional volatiles are almost certainly present in

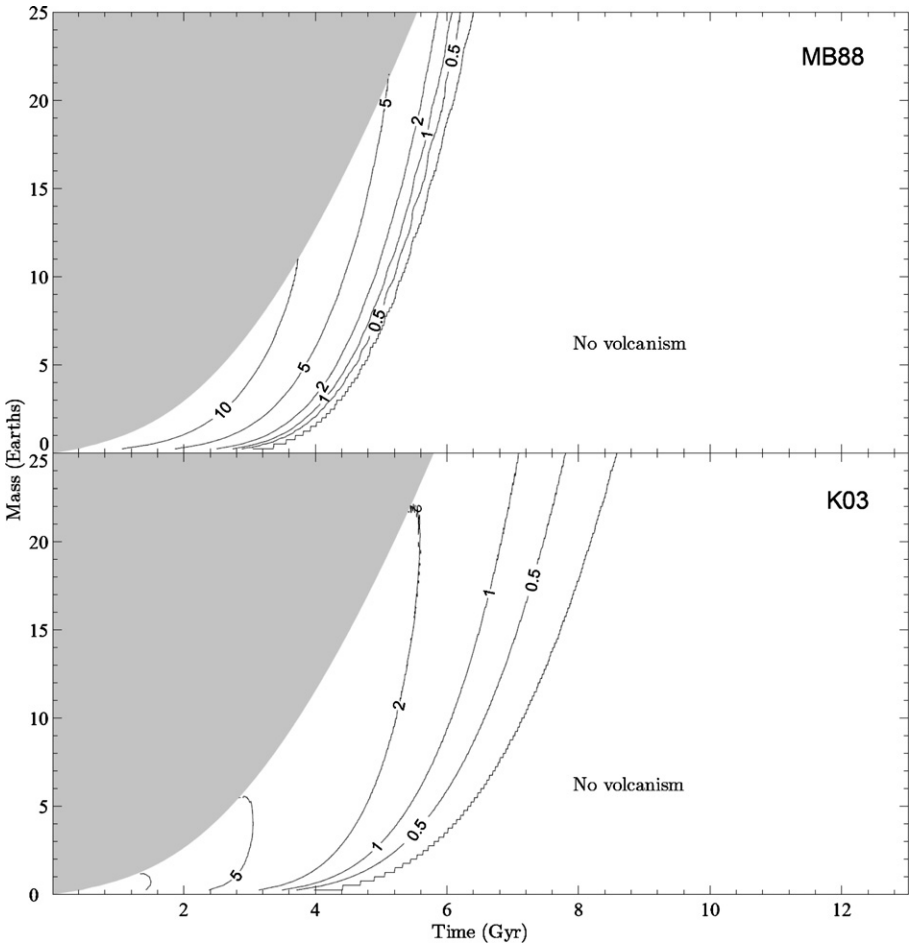

Figure 16. Rate of volcanism on massive Earth-like planets undergoing stagnant lid convection, normalized to calculated rate on a plate-tectonic Earth, for MB88 (top) and K03 (bottom) melting models. Dark gray shaded regions correspond to mantle temperatures too high for a reliable crustal thickness calculation. Contours are at 0, 0.5, 1, 2, 5, and 10 times Earth's rate.

an unmeasured fluid phase), assuming that all mantle fluxing through the melting zone is completely degassed, and ignoring overburden pressure, our model yields 6×10^{13} mol a^{-1} for H_2O and 7×10^{11} mol a^{-1} for CO_2. This is within the range of uncertainty of observational estimates (Oppenheimer 2003). Because our model is not "tuned" to observed rates of volcanism, but only to crustal thickness, this lends some credence to our results for other Earth-like planets.

5.2. Overburden Pressure

The rate of degassing from seafloor volcanoes will also be regulated by the thickness of the volatile overburden. A volatile envelope can have two effects.

1. Through a greenhouse effect, a volatile envelope can raise surface temperatures, and increase partial melting. This is shown for our thermal-equilibrium model in Figure 2. Here, we show the internal temperature needed to drive convection when the surface temperature is 647 K, the critical point of water (q.v. 273 K for the baseline model). In thermal equilibrium, the reduced mantle-surface temperature difference demands more vigorous convection to drive the same heat flux across the upper boundary layer. The increase in mantle temperature is 50–55 K (Figure 2), which has a significant feedback effect on melting (Figure 3). Such high surface temperatures are classically considered to be encountered only for brief intervals on the path to a runaway greenhouse (Ingersoll 1969), but if this catastrophe is suppressed for massive Earths (Pierrehumbert 2007), massive Earths will experience these temperatures for geologically significant intervals. The sign of this feedback is positive; higher mantle temperatures increase crustal thickness, and the associated degassing would enhance the greenhouse effect. We do not consider still higher temperatures, relevant for close-in rocky exoplanets (Gaidos et al. 2007), because plate tectonics is thought to require liquid water.
2. Through overburden pressure, a volatile envelope can suppress degassing (and melting for sufficiently thick volatile layers). Water degassing is readily suppressed by 0.1–0.2 GPa of overburden (Papale 1997), although joint-solubility effects allow some water to degas at higher pressures in association with other gases (Papale 1999). CO_2, an important regulator of climate on the known terrestrial planets, has a solubility of 0.5% GPa^{-1}. Therefore, the overburden pressure provided by 100 km of ocean on a 1 Earth-mass planet is enough to suppress CO_2 degassing from a magma containing 0.5 wt % CO_2. A planet with a massive ocean cannot degas. However, it can regas, provided that hydrous/carbonated minerals pass the line of arcs at subduction zones. This suggests a steady state ocean mass over geodynamic time.

Much more pressure is needed to shut down melting than is needed to shut down degassing (Figure 17). However, numer-

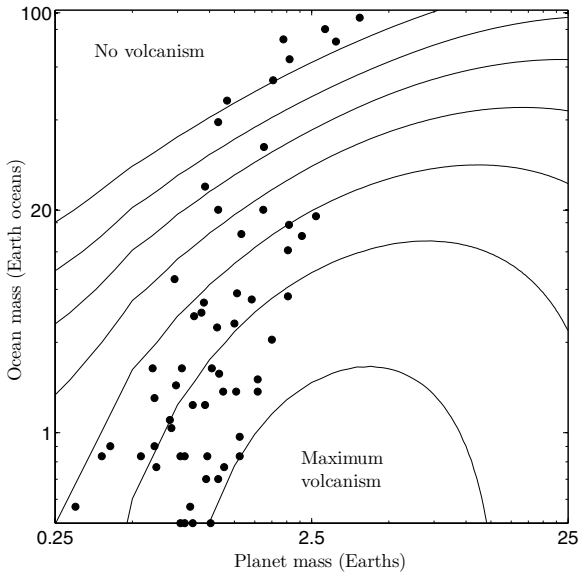

Figure 17. Crustal thickness as a function of planet mass and ocean mass for planets with plate tectonics, after 4.5 Gyr. K03 melting model. Solid lines are contours of crustal thickness at 1 km intervals. Small fluctuations in the contours are interpolation artifacts. Black circles correspond to simulated planets in habitable zone from Raymond et al. (2004, 2006), assuming (following Raymond et al. 2006) that volatiles are partitioned between surface and mantle reservoirs in the same proportions as on Earth. We treat the effect of the volatile overburden on melting as being equivalent to that of a stagnant lid with the same basal pressure.

ical simulations of water delivery during late-stage accretion (Raymond et al. 2004, 2006) produce some planets with the necessary ocean volumes to shut down melting—the stochastic nature of late-scale accretion introduces a great deal of scatter. The largest planets we consider may accrete and retain a significant amount of nebula gas (Ikoma et al. 2001), which would also frustrate melting.

Note that even for an ocean of constant depth, land is unlikely on planets much more massive than Earth. Gravity defeats hypsometry. For example, doubling Earth's gravity would reduce the land area by a factor of 8. This is important for climate-stabilizing feedback loops involving greenhouse-gas drawdown (Walker et al. 1981). Submarine weathering is probably less dependent on surface T than subaerial weathering, so in the case of a water-covered planet we would expect a weaker stabilizing feedback on planet temperature from CO_2–silicate weathering.

5.3. Melt-Residue Density Inversion: Decoupling Melting from Mantle Degassing?

Melts are more compressible than mantle minerals, so at sufficiently high pressures melt will be denser than its residue; for example, mid-ocean ridge basalt becomes denser than garnet at 12.5–19.5 GPa (Agee 1998). If the sinking rate exceeds mantle velocities, these denser melts may accumulate at the base of the mantle (Ohtani & Maeda 2001). Meanwhile, the residue will continue to rise to shallow pressures, where it will eventually generate melt less dense than itself. That melt will segregate, ascend, and form a crust. However, because atmosphere-forming volatiles are highly incompatible, they will partition into the early stage (sinking) melt and erupted melts will be volatile-poor. Generating melt at sufficiently high pressures for the density inversion to come into play requires very high potential temperatures. In our modeling, these are not encountered for planets in plate tectonic mode (except during the first 1 Gyr, which is a transient associated with cooling from our high initial temperature; initial conditions are thus very important). But the density crossover is encountered for >5 $M_\oplus$ and <3 Gyr in stagnant lid mode. We speculate that in these planets, melting is decoupled from mantle degassing.

6. DISCUSSION AND CONCLUSIONS

6.1. Summary of Results

1. *Modest effect of planet mass on temperature and crustal thickness.* Scaling analysis predicts T_m should only be weakly dependent on planet mass (Stevenson 2003). Because of the exponential dependence of viscosity on temperature, modest variation in T_m can accommodate the range of heat flows generated by planets of varying masses. Our more detailed study confirms this, and although the nonlinearity of mantle melting leads to greater variations in crustal thickness, these are still of order unity (Section 3.2; Section 3.3; Figure 5). However, planet mass can determine which mode of mantle convection the planet is in (Section 4), which in turn determines whether melting is possible at all (Section 3.3).
2. *Inhibition of plate tectonics on massive Earths.* Plate buoyancy is an increasingly severe problem for plate tectonics as planet mass increases (Section 4.5). Because early Earth faced the same challenge, geologic fieldwork may determine the threshold beyond which plate tectonics shuts down (Section 4.5). Middle-aged super-Earths may suffer from continental spread, which could choke off plate tectonics (Section 4.4). Shutdown of plate tectonics could place a planet in stagnant lid mode.
3. *Shutdown of melting on old, stagnant lid planets.* All our melting models predict that stagnant lid planets older than Earth cease melting and volcanic activity (Sections 3.3–5, but see caveats in Section 6.2). Therefore, observed volcanism on rocky planets >8 Gya would provide some support for plate tectonics—if and only if tidal heating could be shown to be small. A candidate planetary system has been identified around τ Ceti (Marcy 2002), a 10 Gya star at 3.65 pc, and may provide an early test of this prediction.
4. *Implications for the stability of atmospheres, climate, and habitability.* The atmospheres of Venus, Earth, and Mars were produced by the release of gases dissolved in partial melts, as well as temperature-dependent exchange of volatiles between the atmosphere and surface rocks. Planets lacking dynamos and on close orbits around their parent stars may experience high rates of atmospheric erosion due to stellar winds and coronal mass ejections (Khodachenko et al. 2007), and their atmospheres would persist on main-sequence timescales only if maintained by mantle melting. Under more benign conditions, crust formation may establish the long-term carbon dioxide content of Earth-like atmospheres; CO_2 released in volcanism is sequestered as carbonates produced during the low-temperature weathering of that crust (Walker et al. 1981). Volcanism may underpin the long-term habitability that the fossil record teaches us is a prerequisite for advanced life (Butterfield 2007).

6.2. Overview of Approximations and Model Limitations

In this paper, we assume whole-mantle convection. Layered mantle convection can alter the volcanic history of a planet by

introducing long-term sensitivity to initial thermal conditions. For a phase boundary to form a barrier to flow its Clapeyron slope must be strongly endothermic. Historically, the $sp \rightarrow pv$ transition was thought to have this character but this is now known not to be the case. Deeper phase transitions are either exothermic ($pv \rightarrow ppv$) or very gradual (Seager et al. 2007). In spite of these arguments against layered mantle convection, barriers to flow are possible if stable deep mantle layers arise during or shortly after fractional crystallization of the primordial magma ocean. Although CMB pressures reach 14 Mbar for 10 $M_\oplus$ and 40 Mbar for 25 $M_\oplus$, we have not considered metalized silicates (Umemoto et al. 2006), nor the possibility that lower-mantle convection is extremely sluggish (even isoviscous; Fowler 1983) due to low homologous temperatures, nor pressure-dependent viscosity (Papuc & Davies 2008). Our parameterized treatment of mantle convection assumes the solid state and is inappropriate for very high temperatures, when the greater part of the lithosphere is underlain by a magma ocean. For almost all cases, however, the transition to a magma ocean takes place at temperatures beyond the range of validity of our melting models, so magma ocean development is not the limiting consideration in interpreting our results.

Our model does not consider tidal heating, which may be important for Earth-like planets on close eccentric orbits about low-mass stars (Jackson et al. 2008), nor does it take into account the energetics of the core (Nimmo 2007). Because the magnitude of core cooling is set by mantle cooling, core energetics only dominate mantle thermal evolution in Earth-like planets as $t \rightarrow \infty$ and $H \rightarrow 0$. Surface temperature is assumed to be constant, which is likely to be a good approximation except for close-in exoplanets with thin atmospheres in a 1:1 spin-orbit resonance (Ganesan et al. 2008).

All our melting models show "solidus rollover" at high P—that is, $\frac{T_{\rm sol}}{P} \rightarrow \frac{\partial V}{\partial S}$. As a consequence, plots of X versus P at high T_p have a long, thin high-pressure tail, and the pressure of first melting diverges at finite T_p. Although solidus rollover is a real effect, resulting from the greater compressibility of silicate melts versus solids (Ghiorso 2004), infinite pressures of first melting are unphysical. In particular, phase transitions near 14 GPa introduce unmodeled kinks of the solidus. To sidestep the solidus rollover problem, we truncate our melting integration at 8 GPa, and do not plot model output where melting models predict nonzero X at 8 GPa. But this solution has costs: (1) we cannot model hot planets (grayed-out regions in Figures 5 and 7), and (2) because pressure at first melting is so sensitive to solidus rollover, we have little confidence in our model output for the rate of processing of the mantle through the melt zone. Melting models calibrated to higher pressures and temperatures would remove this impediment to progress. One such model (xMELTS), based on a high-pressure equation-of-state for silicate liquids (Ghiorso 2004), will soon become available (Ghiorso et al. 2007). Because crustal production rate is proportional to the integral under the curve of X versus P, rather than the pressure at which $X = 0$, it is much less sensitive to this problem. Representing the solidus as a straight line in T–P space (Papuc & Davies 2008) is geologically not realistic, but has the advantage that both crustal thickness and the pressure of first melting are finite for all T_p.

We calculate crustal thickness as the integral of melting fraction from the surface to great depth. In plate tectonic mode, this corresponds to the observable (seismically defined) crustal thickness. But in stagnant lid mode, the observable crustal thickness need not be the same everywhere (because melting will only occur above mantle upwellings). Also, the observable crustal thickness may be everywhere greater than the integral of melting fraction from the surface to great depth, because crust generated in previous melting events is located directly underneath "fresh" crust. This situation is described in the context of Io by Moore (2001). On stagnant lid planets, volcanism may be episodic (as on Mars; Wilson et al. 2001) and absent for long periods. This means that an observed lack of compounds with a short photochemical lifetime would not preclude a high level of volcanic activity averaged over a sufficiently long period ($\gtrsim 10^{\sim 8}$ yr). Volcanism is not the only possible source of degassing. Metamorphic decarbonation (Bickle 1996), and the episodic release of deep-seated volatiles as on the Moon (Gorenstein & Bjorkholm 1973), could permit (low) rates of degassing on nonvolcanic worlds.

By assuming that all melt reaches the surface, we have ignored the distinction between extrusion and intrusion. However, extrusion can alter the reflectance properties of the planet without sustaining an atmosphere—consider the Moon—and it may eventually be possible to discriminate between the two possible fates for melt.

6.3. Comparison with Solar System Data

6.3.1. Thermal Evolution, with an Emphasis on Earth

Four decades since plate tectonics became widely accepted, geologists have not determined the detailed thermal history of the Earth, neither have we even produced a model that satisfyingly accounts for the few data points in hand. The model of Korenaga (2006, taking a parameterized approach) may be an exception, but this model assumes that present-day observed averages are valid for the past, and is probably not portable to other Earth-like planets. Complicating the picture are two sharp-edged lower mantle anomalies mapped by seismic tomography under Africa and the S. Pacific, which are likely distinct in composition and radiogenic-element density from the rest of the mantle and which may be persistent, ancient features that have interfered in mantle convection since more than 2.5 Gyr ago. Their origin is unknown (Garnero & McNamara 2008). Geoneutrino detectors will break some of these degeneracies before 2020, and continued field mapping of ancient tectonic features will sharpen the history of past dynamics of plate deformation (Condie & Pease 2008). But using simple models and making changes along one dimension only—the approach taken here—is still a meaningful approach because the more complex models introduce many more free parameters, and it is not clear how these free parameters vary with mass. By contrast, our approach involves only one "tuning" parameter, the offset $T_m - T_p$.

The situation for the other terrestrial planets—single plate planets with stagnant lithospheres—is in many ways better. Parameterized cooling fits all the observations. This is not just because of a lack of data: stagnant lid planets seem to be truly simpler, and the relevant fluid physics is probably better understood than the "viscoelastoplastic plus damage" phenomenology needed to accommodate the observed geological motions of the Earth's plates. On Earth, mantle heat loss is largely by conduction aided by hydrothermal convection at mid-ocean ridges, but mantle heat loss on stagnant lid planets should be less sensitive to the details of surface deformation.

The degree to which the mantle cools over geological time depends on the activation energy for deformation of mantle rock, which is known only imprecisely (Karato 2008). We take

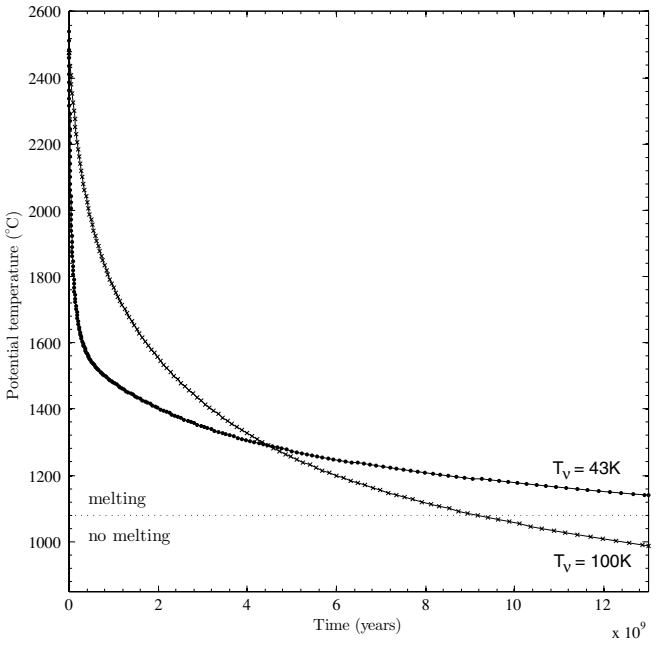

Figure 18. Effect of changing activation energy for temperature-dependent viscosity on thermal evolution. Turcotte & Schubert (2002) radiogenic-element complement ($M_\oplus = 1$). Mantle temperatures are adjusted to produce 7 km thick crust under MB88 at 4.5 Gyr. Dots correspond to results with $T_\nu = 43$ K. Stars correspond to results with $T_\nu = 100$ K. Note that the cooling rate at 4.5 Gyr is 71 K Gyr^{-1} for $T_\nu = 100$ K, more than double that for $T_\nu = 43$ K (33 K Gyr^{-1}). Cessation of melting (dashed line) occurs around 9 Gyr for $T_\nu = 100$ K, but takes longer than the age of the universe for $T_\nu = 43$ K.

$T_\nu \cong 43$ K, for which $A_0 = 7 \times 10^4$ K, giving an order-of-magnitude viscosity change for each 100 K temperature increment (although T_ν could be as high as 100 K; Sleep 2007). This is conservative (but not necessarily more correct) in terms of the effect of mass on temperature, because small values of T_ν allow mass (heat flux) variations to be accommodated by small changes in temperature (Figure 18).

Continents affect thermal evolution (Section 4.4). However, continent growth and survival is not well understood. Hydration of the oceanic crust at mid-ocean ridges, and subduction of this H_2O, is probably required for continental growth (Campbell & Taylor 1983). There is geological and isotopic evidence for episodic continental growth (Condie & Benn 2006). Durable continents may require photosynthetic life both in the oceans (Rosing 2006) and on land (Lee et al. 2008). None of these effects are straightforward to model. So, though excessive continental surface area and radiogenic-element sequestration both have the potential to throttle our predicted increase in mantle melting on high-mass Earths, we consider this only a tentative prediction.

6.3.2. Melting: Constraints from Venus, Mars, Io, and the Moon

If massive Earth-like planets are in heat-pipe mode for ~1 Gya (Section 4.2), a substantial fraction of the census of nearby massive Earth-like planets would be in heat-pipe mode. And if Io is any guide (e.g., Lopes & Spencer 2007), dramatic spatial and temporal variations in thermal emission should be present. However, the relatively slow cooling in our thermal evolution model is inappropriate for magma oceans (Sleep 2007), because our parameterization of viscosity does not include the 15 order-of-magnitude decrease associated with melting. Planets with $Mo > 1$ are likely to cool quickly to $Mo < 1$; we suspect that Io-type cooling is unsustainable for geologically significant periods without a nonradiogenic source of energy.

Our melting model is tuned to Earth only, but fits Venus observations reasonably well. With the MB88 model, our calculations show that volcanism on a planet in stagnant lid mode and with Venus' mass ($M_\oplus = 0.85$) will cease after 3.9 Gyr, which is consistent with observations (Schaber et al. 1992).

However, when decompression melting of mantle material at background temperatures cannot sustain volcanism on Earth-like planets undergoing whole-mantle convection, other mechanisms may take over. Plumes rising from the CMB, or from a compositional interface within the mantle, can have temperatures up to several hundred degrees greater than that of passively upwelling mantle. This requires a more detailed treatment of thermal evolution than we have taken in this paper, and could be the basis of a more detailed study.

In particular, Mars' continuing—although fitful and low-rate—volcanic activity (Borg & Drake 2005) indicates that volcanic activity can continue on planets in stagnant-lid mode for longer than our simple models predict, perhaps as the result of plumes in a compositionally layered mantle (Wenzel et al. 2004) or a thick, thermally insulating crust (Schumacher & Breuer 2007). On Venus, mantle fluxing by sinking delaminated lithosphere has been proposed as a mechanism that would allow volcanism to continue through to the present day (Elkins-Tanton et al. 2007), although there is no robust evidence of ongoing volcanism. Continued solar system exploration is needed if we are to fully exploit nearby data points to understand the geodynamic window for life.

Many of the ideas discussed here are drawn from the conversation of Dave Stevenson, whose support for the early stages of this project was invaluable. We thank Nick Butterfield, Rhea Workman, Brook Peterson, Norm Sleep, and Itay Halevy for their productive suggestions. We acknowledge support from the NASA Astrobiology Institute. E.K. acknowledges support from the Berkeley Fellowship and a Caltech Summer Undergraduate Research Fellowship.

REFERENCES

Afonso, J. C., Ranalli, G., & Fernàndez, M. 2007, Geophys. Res. Lett., 34, L10302
Agee, C. B. 1998, Phys. Earth Planet. Inter., 107, 63
Anders, E., & Grevesse, N. 1989, Geochim. Cosmochim. Acta, 53, 197
Best, M. G., & Christiansen, E. H. 2001, Igneous Petrology (Oxford: Wiley-Blackwell)
Bickle, M. J. 1996, Terra Nova, 8, 270
Borg, L. E., & Drake, M. J. 2005, J. Geophys. Res., 110, E12S03
Bucher, K., & Frey, M. 2002, Petrogenesis of Metamorphic Rocks (7th ed., Berlin: Springer)
Butterfield, N. J. 2007, Palaeontology, 50, 41
Campbell, I. H., & Taylor, S. R. 1983, Geophys. Res. Lett., 10, 1061
Carlson, R. L., & Herrick, C. N. 1990, J. Geophys. Res.B, 95, 9153
Cescutti, G. 2008, A&A, 481, 691
Chen, Z., Zhang, J., Chen, Y., Cui, W., & Zhang, B. 2006, Astrophys. Space Sci., 306, 33
Cloos, M. 1993, Geol. Soc. Am. Bull., 105, 715
Condie, K. C., & Benn, K. 2006, in Archean Geodynamics and Environments, ed. K. Benn et al. (Washington, DC: AGU), 47
Condie, K. C., & Pease, V. (ed.) 2008, When Did Tectonics Begin on Planet Earth? (Special paper 440; Boulder, CO: Geol. Soc. Am.)
Davies, G. F. 1992, Geology, 20, 963
Davies, G. F. 2007, Geophys. Geochem. Geosyst., 8, Q04006
de Pater, I., & Lissauer, J. 2001, Planetary Sciences (Cambridge: Cambridge Univ. Press)
Elkins-Tanton, L. T., & Seager, S. 2008a, ApJ, 685, 1237
Elkins-Tanton, L. T., & Seager, S. 2008b, ApJ, 688, 628

Elkins-Tanton, L. T., Smrekar, S. E., Hess, P. C., & Parmentier, E. M. 2007, J. Geophys. Res., 112, E03005
Fowler, A. 1983, J. Geophys. Res., 53, 42
Frebel, A. 2008, in ASP Conf. Proc. 393, New Horizons in Astronomy: Frank Bash Symp. 2007, ed. A. Frebel et al. (San Francisco, CA: ASP), 63
Gaidos, E. J. 2000, Icarus, 145, 637
Gaidos, E., Haghighipour, N., Agol, E., Latham, D., Raymond, S., & Rayner, J. 2007, Science, 318, 210
Ganesan, A. L., Elkins-Tanton, L. T., & Seager, S. 2008, Proc. Lunar Planet. Sci. Conf., 39, 1368 (Houston, TX: Lunar and Planetary Institute) (CD-ROM)
Garnero, E. J., & McNamara, A. K. 2008, Science, 320, 626
Ghiorso, M. S. 2004, Am. J. Sci., 304, 811
Ghiorso, M. S., Hirschmann, M. M., & Grove, T. L. 2007, in AGU Fall Meeting, abstract V31C-0608
Ghiorso, M. S., Hirschmann, M. M., Reiners, P. W., & Kress, V. C. 2002, Geophys. Geochem. Geosyst., 3, 1030
Gorenstein, P., & Bjorkholm, P. 1973, Science, 179, 792
Grasset, O., & Parmentier, E. M. 1998, J. Geophys. Res., 103, 18171
Ida, S., & Lin, D. N. C. 2004, ApJ, 604, 388
Ikoma, M., Nakazawa, K., & Emori, H. 2001, ApJ, 537, 1013
Ingersoll, A. P. 1969, J. Atmos. Sci., 26, 1191
Jackson, B., Greenberg, R., & Barnes., R. 2008, ApJ, 678, 1396
Juteau, T., & Maury, R. 1999, The Oceanic Crust, From Accretion to Mantle Recycling (Chichester: Springer-Praxis)
Karato, S. 2008, Deformation of Earth Materials (Cambridge: Cambridge Univ. Press)
Katz, R. F., Spiegelman, M., & Langmuir, C. H. 2003, Geochem. Geophys. Geosyst., 4, 1073
Khodachenko, M. L., et al. 2007, Astrobiology, 7, 167
Korenaga, J. 2006, in Archean Geodynamics and Environments, ed. K. Benn et al. (Washington, DC: AGU), 7
Korenaga, J. 2008, Rev. Geophys., 46
Kuchner, M. J., & Seager, S. 2005, arXiv:astro-ph/0504214
Langmuir, C. H., Klein, E. M., & Plank, T. , in Mantle Flow and Melt Generation at Mid-Ocean Ridges, ed. J. P. Morgan et al. (Washington, DC: AGU), 183
Lee, C.-T. A., Morton, D. M., Little, M. G., Kistler, R., Horodyskyj, U. N., Leeman, W. P., & Agranier, A. 2008, Proc. Natl Acad. Sci., 105, 4981
Lenardic, A., Jellinek, A. M., & Moresi, L.-N. 2008, Earth Planet. Sci. Lett., 271, 34
Lenardic, A., Moresi, L.-N., Jellinek, A. M., & Manga, M. 2005, Earth Planet. Sci. Lett., 234, 317
Lopes, R. M. C., & Spencer, J. R. 2007, Io after Galileo (Berlin: Springer)
Loyd, S. J., Becker, T. W., Conrad, C. P., Lithgow-Bertelloni, C., & Corsetti, F. A. 2007, Proc. Natl Acad. Sci., 104, 14266
Lyubetskaya, T., & Korenaga, J. 2007, J. Geophys. Res., 112, B03212
Marcy, G. W. 2002, http//exep.jpl.nasa.gov/ao(underscore)support/marcy.pdf
McKenzie, D. 1984, J. Petrol., 25, 713
McKenzie, D., & Bickle, M. J. 1988, J. Petrol., 29, 625
McKenzie, D., Jackson, J., & Priestley, K. 2005, Earth Planet. Sci. Lett., 233, 337
Moore, W. B. 2001, Icarus, 154, 548
Moore, W. B. 2003, J. Geophys. Res., 108, 5096
Newsom, H. E. 1995, in Global Earth Physics: A Handbook of Physical Constants, ed. T. J. Ahrens (Washington, DC: AGU), 159
Nimmo, F. 2007, in Treatise on Geophysics Vol. 8, ed. G. Schubert (Amsterdam: Elsevier), 31
Ohtani, E., & Maeda, M. 2001, Earth Planet. Sci. Lett., 193, 69
O'Neill, C., & Lenardic, A. 2007, Geophys. Res. Lett., 34, L19204
Oppenheimer, C. 2003, in Treatise on Geophysics Vol. 3, ed. H. D. Holland & K. K. Turekian (Amsterdam: Elsevier), 123
Papale, P. 1997, Contrib. Mineral. Petrol., 126, 237
Papale, P. 1999, Am. Mineral., 84, 477
Papuc, A. M., & Davies, G. F. 2008, Icarus, 195, 447
Pierrehumbert, R. 2007, AGU Fall Meeting, abstract P54A-08
Pont, F., & Eyer, L. 2004, MNRAS, 351, 487
Prantzos, N., & Silk, J. 1998, ApJ, 507, 229
Raymond, S. N., Quinn, T., & Lunine, J. I. 2004, Icarus, 168, 1
Raymond, S. N., Quinn, T., & Lunine, J. I. 2006, Icarus, 183, 265
Ringwood, A. E. 1991, Geochim. Cosmochim. Acta, 55, 2083
Rivera, E. J., Lissauer, J. J., Paul Butler, R., Marcy, G. W., Vogt, S. S., Fischer, D. A., Brown, T. M., & Laughlin, G. 2005, ApJ, 634, 625
Rosing, M. T., Bird, D. K., Sleep, N. H., Glassley, W., & Albarede, F. 2006, Palaeogeogr. Palaeoclimatol. Palaeoecol., 232, 99
Schaber, G. G., et al. 1992, J. Geophys. Res., 97, 13257
Schubert, G., Turcotte, D. L., & Olsen, P. 2001, Mantle Convection in the Earth and Planets (Cambridge: Cambridge Univ. Press)
Schumacher, S., & Breuer, D. 2007, Geophys. Res. Lett., 34, L14202
Seager, S., Kuchner, M., Hier-Majumder, C., & Militzer, B. 2007, ApJ, 669, 1279
Sleep, N. H. 2000, J. Geophys. Res., 105, 17563
Sleep, N. H. 2007, in Treatise on Geophysics Vol. 9., ed. G. Schubert (Amsterdam: Elsevier), 145
Sleep, N. H., & Zahnle, K. H. 2001, J. Geophys. Res., 106, 1373
Smith, P. M., & Asimow, P. D. 2005, Comptes Rendus Geoscience, 6
Stevenson, D. J. 2003, C. R. Acad., 335, 99
Tozer, D. C. 1970, Phys. Earth Planet. Inter., 2, 393
Turcotte, D., & Schubert, G. 2002, Geodynamics (2nd ed.; Cambridge: Cambridge Univ. Press)
Umemoto, K., Wentzkovitch, R. M., & Allen, P. B. 2006, Science, 311, 983
Valencia, D., O'Connell, R. J., & Sasselov, D. D. 2006, Icarus, 181, 545
Valencia, P. D., O'Connell, R. J., & Sasselov, D. D. 2007, ApJ, 670, L45
Vlaar, N. J., van Keken, P. E., & van den Berg, A. P. 1994, Earth Planet. Sci. Lett., 121, 1
Walker, J. C. G., Hays, P. B., & Kasting, J. F. 1981, J. Geophys. Res., 86, 9776
Wenzel, M. J., Manga, M., & Jellinek, M. A. 2004, Geophys. Res. Lett., 31, L04702
White, R. S., Minshull, T. A., Bickle, M. J., & Robinson, C. J. 2001, J. Petrol., 42, 1171
Wilson, L., Scott, E. D., & Head, J. W. 2001, J. Geophys. Res., 106, 1423
Workman, R. K., & Hart, S. R. 2005, Earth Planet. Sci. Lett., 231, 53